Adapting the Landscape? Climate Extremes and Land Use changes

Giulia Tozzi

Working Paper No. 999 December 2025 ISSN 1473-0278

School of Economics and Finance

Queen Mary University of London

Adapting the Landscape? Climate Extremes and Land Use changes

Giulia Tozzi*
Queen Mary University of London

December 18, 2025

Abstract

This paper investigates whether societies adapt to climate shocks by modifying land use over time. I develop a hydrometeorological framework that links extreme precipitation to flooding via antecedent moisture and drainage capacity, and use it to interpret reduced-form effects of extreme-precipitation years on land-use shares and local economic activity. Focusing on India from 2001 to 2010, I combine district-year satellite data with a difference-in-differences event-study design that traces outcomes up to five years after a shock and constructs model-implied cumulative effects under repeated exposure. I find no statistically discernible medium-run changes in cropland, forest cover, built-up shares, or night-time light intensity following extreme-precipitation years. When averaging over the first four post-shock years, I can rule out shifts larger than about 0.1 residual standard deviations of within-district variation over time in cropland, built-up areas, and night-time lights. Overall, these findings indicate rigid spatial adaptation in one of the world's most climate-exposed settings.

Keywords: Climate Exposure, Climate Adaptation, Land Use, Spatial Adaptation, India.

* School of Economics and Finance, Queen Mary University of London (QMUL), Mile End Road, London, E1 4NS. Email: g.tozzi@qmul.ac.uk, Webpage: https://sites.google.com/view/giuliatozzi/

I would like to thank my supervisors Jonathan de Quidt and Lucie Gadenne. I am grateful to Cristina Cibin, Andrea Smurra, Marco Castelluccio and fellow researchers at the Institute for Fiscal Studies for their help and advice. I gratefully acknowledge funding towards my doctoral studies by QMUL and AMSE. All errors remain my own.

1 Introduction

Climate change has increased the frequency and severity of extreme weather events globally, imposing substantial economic and social risks. According to the Intergovernmental Panel on Climate Change (IPCC), global record-breaking rainfall events increased by 12% during 1981–2010 relative to expectations under natural multi-decadal climate variability. In addition, both precipitation intensity and variability are projected to rise, increasing vulnerability to floods and rainfall extremes (Lehmann et al., 2015; Intergovernmental Panel on Climate Change (IPCC), 2022; Intergovernmental Panel On Climate Change (IPCC), 2023). In the case of India, annual flood-related economic losses exceed $3 billion[1], which constitute 10% of the global flood-induced economic losses (Roxy et al., 2017). With more than 1.4 billion people primarily depending on agriculture and rapid population growth, India faces a severe threat to its socio-economic stability from the increasing frequency of these events (Ghosh et al., 2012; Roxy et al., 2017; Tellman et al., 2021; Raghuvanshi et al., 2025; Chuphal et al., 2025).

While previous research highlights technology adoption, migration, and infrastructure improvements as adaptation channels, land-use systems are a key determinant of how climate risk is distributed and a central lever for climate policy. From an economic perspective, land use and land tenure jointly shape both exposure—by determining where people, firms, and infrastructure are located relative to hazards—and vulnerability, by governing which assets, production technologies, and ecosystem services are in harm's way when a shock hits. Because land is a slow-moving, quasi-fixed factor, adjustments in land allocation, settlement patterns, and land-cover composition constitute a distinct, potentially powerful, but often politically and institutionally constrained adaptation margin. Yet systematic evidence on how land-use patterns respond to climatic extremes remains scarce.

This paper investigates whether land systems in India adapt to climate-driven intensification of extreme events. Specifically, I examine whether exposure to climatic extremes induces systematic shifts in economic activity and land allocation among cropland, forest cover, and urban (built-up) uses.

The analysis uses high-resolution, harmonised satellite data covering Indian districts from 2001 to 2010 and examines both short- and medium-term dynamics. I construct an annual

[1] "India has witnessed several extreme precipitation events in the past that caused catastrophes. The 2023 Himachal Pradesh extreme precipitation event claimed around 120 casualties and caused extensive damage to infrastructure (Gupta et al., 2024), while the 2005 Mumbai event affected over 20 million people, resulting in more than 1,000 deaths (Ranger et al., 2011). The 2014 Kashmir floods caused nearly 277 fatalities in India (I. H. Malik, 2022), and the 2013 Uttarakhand event led to over 6,000 deaths and economic losses exceeding $3.8 billion (Kumar, 2013)." (Chuphal et al., 2025)

district-level panel for 2001–2010 by integrating high-resolution satellite imagery with remotely sensed proxies for land use and economic activity. The dataset has three components. First, extreme-precipitation events are identified using NASA's GPM IMERG Final product, and a district is treated if monthly rainfall exceeds 1,000 mm at least once within the calendar year. Second, annual land-use estimates come from the HILDA spatial reconstruction for India, which combines district inventories with 100-meter imagery to produce yearly maps of cropland, forest cover, and built-up areas. Third, economic activity is proxied by harmonised night-time lights from DMSP-OLS and VIIRS.

Conceptually, extreme precipitation affects outcomes through two channels: (i) direct rain impacts (waterlogging, erosion, drainage stress) and (ii) translation into floods when capacity constraints bind. To clarify coefficient interpretation, I develop a hydrometeorological framework that maps extreme precipitation to flooding via a probabilistic link governed by antecedent moisture and routing/drainage capacity.

I then estimate a district–year difference-in-differences event-study specification with distributed lags of extreme-precipitation years, which traces the path of land use and economic activity from the year of an extreme-precipitation shock up to five subsequent years, comparing exposed and non-exposed districts after conditioning on district and year fixed effects. Under a linear additivity assumption, I use the estimated impulse responses to construct model-implied cumulative effects for sequences of repeated shocks.

The analysis reports three main sets of results. First, the distributed-lag estimates indicate no statistically discernible short-run or medium-run changes in cropland, forest cover, or built-up shares following extreme precipitation. In the average post-treatment window, I can rule out shifts exceeding about 0.07 residual standard deviations for cropland; for built-up land and night-time lights, the bounds are about 0.07 and 0.12 residual standard deviations; for forest cover, uncertainty remains wider at about 0.25 residual standard deviations. These standard deviations refer to within-district interannual fluctuations after conditioning on district and year fixed effects and are small relative to mean levels: for cropland, forest, and built-up land, the residual standard deviations are only about 1–6 percent of their sample means. For cropland, built-up land, and night-time lights, the 95 percent confidence-interval half-widths therefore correspond to at most about one-tenth of this remaining within-district variation, so any systematic medium-run response along these margins, if present, must be smaller than roughly 0.1 residual standard deviations. Results are robust to a looser definition of extreme-precipitation years, which classifies a year as extreme if at least one month records precipitation exceeding 500 mm. The small within-district residual variation and the narrow confidence

intervals indicate that land use is a rigid adaptation margin: even under repeated shocks, districts do not reallocate land in ways that are detectable in the data. Second, from a mechanism perspective, a validation regression shows that the precipitation-based treatment captures realized flooding: an extreme-precipitation year is associated with a roughly 41% increase in district flood occurrence relative to the sample mean. Third, as a benchmark, I revisit the India case study in Kocornik-Mina et al. (2020) using a similar district–year design but a more inclusive definition of floods and harmonised night-time lights. While they find small and imprecise effects, I find that log night-time lights fall by 0.050 in flood years and by 0.069 one year after an extreme-precipitation event, both statistically significant at the 1% level, with no evidence of longer-run effects. These estimates sharpen the imprecise Indian coefficients reported by Kocornik-Mina et al. (2020) while remaining consistent with their central global conclusion that large floods generate short-run disruptions but no persistent losses in local economic activity.

Globally, roughly half of the mitigation and adaptation measures pledged under the Paris Agreement are land-related, and about 40 percent of those require direct physical access to land (Torhonen, 2024). These land-intensive measures—ranging from climate-resilient infrastructure and renewable-energy siting to forest conservation, coastal protection, and urban upgrading—are concentrated in rural and forest landscapes and on the fringes of rapidly growing cities and coastal zones, where tenure insecurity, informality, and poverty are most prevalent (Chen, 2024). Understanding whether land-use patterns adjust to extreme events is therefore key for assessing climate vulnerability and for designing land, infrastructure, and tenure policies that can enable spatial reallocation away from high-risk locations and towards more resilient land uses.

India provides an especially relevant setting for studying spatial adaptation to climate extremes. As Rexer and Sharma (2024) reports, the country faces both growing exposure and vulnerability to such events: the long-run impacts of climate change are projected to reduce farm yields by at least 25 percent (Guiteras, 2009), while manufacturing output declines by around 2 percent per additional degree Celsius of warming (Somanathan et al., 2021). Cyclones alone destroy an average of 2.2 percent of firms' fixed assets (Pelli et al., 2023). Although some evidence documents adaptive behavior—such as investments in irrigation or crop switching (Taraz, 2017)—such adjustments often recover only a small fraction of climate-related losses. The modest effects of flood-tolerant rice varieties on yields further emphasize the limits of technical fixes in the absence of broader transformation (Dar et al., 2013). Indeed, structural shifts out of agriculture in India have been shown to reduce heat-related losses by 69 percent

from 2001 to 2007 (Colmer, 2021). Against this background, my findings of limited land-use adaptation suggest that spatial and structural inertia remains a critical constraint on India's climate resilience.

From a policy perspective, the absence of spatial reallocation in response to extreme precipitation implies that incremental adaptations at the margin—such as modest changes in crop choice or local infrastructure repairs—are unlikely to suffice given the scale of climate challenges. In light of evidence that a large share of climate actions require access to land and are concentrated in high-risk, tenure-insecure areas, these results point to rigid land-use systems as a core constraint on climate resilience. Policies that strengthen land administration and tenure security, clarify rights and responsibilities in peri-urban and high-risk zones, and reduce frictions in land, labor, and capital markets are likely necessary to enable spatial reallocation—whether through safer siting of infrastructure, expansion of urban land away from floodplains, or protection and restoration of forests. If current land systems and production structures remain rigid, the economic burden of climate shocks will persist or intensify, with the poorest households disproportionately trapped in high-exposure locations.

This paper contributes to two streams of economic literature.
First, it adds to research assessing the economic consequences of climate shocks. Studies show that higher temperatures reduce agricultural productivity and growth in developing countries (Dell et al., 2012, 2014), increase mortality in both rich and poor contexts (Deschênes and Greenstone, 2011; Burgess et al., 2013; Carleton et al., 2022), and disrupt labor markets and productivity through reallocation and pollution exposure (Khanna et al., 2025; Liu et al., 2023). My paper connects to this strand by shifting attention from outcomes such as productivity, mortality, or political participation to land systems, examining whether extreme precipitation affects the allocation of land across agricultural and non-agricultural uses.

Second, it contributes to the literature examining whether and how societies adapt to climate change. Evidence shows that farmers respond through irrigation, water access, and trade (Deschênes and Greenstone, 2007; Hornbeck and Keskin, 2014; Costinot et al., 2016), mortality from heat declines with the spread of air conditioning (Barreca et al., 2016), positive rainfall shocks expand non-agricultural employment (Emerick, 2018), and exposure to extreme heat alters political participation (Amirapu et al., 2022). Additional work highlights irrigation and groundwater as buffers to drought (Taraz, 2017), railroads and openness as safeguards against famine (Burgess and Donaldson, 2010; Burgess and Donaldson, Dave, 2017), and directed innovation, learning, and sectoral labor shifts as resilience channels, though residual damages often remain (Burke and Emerick, 2016; Kala, 2019; Blakeslee et al., 2020; Moscona and Sastry,

2023; Hultgren et al., 2025). Within this broader literature, a more specific line of work examines how climate shocks shape land use, migration, and urbanization. Studies show that infrastructure, government intervention, and liquidity constraints mediate responses to extreme events (Brooks and Donovan, 2020; Grosset-Touba et al., 2024; Hsiao, 2025; Cattaneo and Peri, 2016; Bazzi, 2017; Burzyński et al., 2022), while large floods and rising temperatures often display negligible effects on structural transformation and urbanization in Sub-Saharan Africa (Henderson et al., 2017) and India (Kocornik-Mina et al., 2020; Liu et al., 2023). My paper contributes to this broader adaptation literature—and in particular to the sub-strand on land use and mobility—by testing an underexplored margin—local spatial reallocation of land use. Using evidence on India and exogenous satellite-based measures of extreme precipitation, I show that even under both isolated and recurrent shocks cropland, forest, and urban land shares remain largely unchanged. The contribution is the *precision* of these null effects. This complements prior work by documenting the rigidity of spatial adaptation in one of the world's most climate-exposed settings.

2 Background and Data

This section describes the institutional and environmental context and the main data sources. This paper relies on a combination of remote-sensing satellite imagery (precipitation and night-lights) and novel gridded datasets (land use and floods). The data are geoprocessed at the district–year level for 2001–2010. Table 1 provides summary statistics for the main variables. The panel comprises roughly 742 districts observed over 10 years. On average, districts are 59% cropland, 24% forest, and 3.8% built-up (the remainder being other covers), with substantial cross-district dispersion—particularly for built-up areas. Between 27% and 29% of district–years experience an extreme precipitation or flood event.

2.1 Land Use

India's population rose from 361 million in 1951 to 1,221 million at the 2011 census, driving substantial environmental change. Increasing population density and a changing economy have resulted in urban expansion, while India's Green Revolution, initiated in the mid-1960s to achieve food security, transformed natural vegetation and rainfed agriculture into intensively managed systems (Moulds et al., 2018). Land use change[2] affects biodiversity and ecosystem

[2]Land use and land cover are closely related but conceptually distinct concepts. According to FAO (2000), land cover refers to the "observed (bio)physical cover on the earth's surface," whereas land use denotes the

services and is a major driver of environmental change, influencing the surface energy and water balance and global biogeochemical cycles. Tian et al. (2014) report that between 1980 and 2010 built-up areas expanded rapidly to accommodate population growth, while cropland expansion to increase food production often came at the expense of forests and natural vegetation. Forest cover remains below the minimum standards set by the National Forest Policy of 1988—33% in plains and 66% in hilly areas—posing concerns for erosion and ecosystem degradation. India's urban population is projected to increase by 273 million people by 2050, with large cities already facing ecological challenges such as deterioration of ecological spaces, loss of ecosystem services, and the emergence of urban heat islands (Das et al., 2024).

I use land-use data from Moulds et al. (2018), the first publicly available, high-resolution reconstruction of Indian land use and land-cover change until 2010. Previous global products such as HYDE or Earthstat relied on state- or national-level aggregates and assumed a static spatial distribution of land use over time, obscuring district-level heterogeneity in the pace and direction of change. By contrast, Moulds et al. (2018) incorporate annual district-level inventory data to capture localized dynamics and allocate them across space using a statistical model informed by biophysical and socioeconomic drivers. The result is a gridded dataset at 100-meter resolution that better represents historical land use during a period of rapid demographic and economic change. The dataset is generated by combining district-level inventories with satellite-based maps and covariates using the Historic Land Dynamics Assessment (HILDA) land change model. Annual land use and land cover data from 1960 to 2010 are drawn from two main sources: Indiastat and the ICRISAT Village Dynamics in South Asia (VDSA) project, both ultimately originating from the Directorate of Economics and Statistics of India's Ministry of Agriculture. These inventories report the extent of land use classes aggregated at the district level. Observed remote-sensing maps for 1985, 1995, and 2005 are used as reference conditions and for calibration, ensuring consistency between modeled and observed totals at the district level. The inventories and satellite maps employ different classification schemes, which are harmonised into a simplified set of categories suitable for modeling. The final dataset distinguishes cropland, forest, grassland, shrubland, wasteland, barren land, and urban land, with water, snow, and ice included as constant categories. Urban areas are estimated from non-agricultural land uses in the inventory data and scaled to match the observed extent in 2005, while barren land functions as the residual category to which remaining pixels are allocated once other categories are assigned. This hierarchy reflects the assumed socioeconomic

arrangements, activities, and inputs through which people manage, modify, or maintain a given land cover type. This definition highlights the direct link between biophysical features and human actions. For simplicity, I use the term land use throughout the paper.

value of land uses, with expansion of higher-value uses such as urban or cropland occurring at the expense of lower-value classes such as wasteland or barren land.

In the analysis, I focus on three categories that represent the agricultural, resource, and urban dimensions of land change: cropland, forest, and built–up areas. These classes capture the most relevant dynamics for examining adaptation to climate extremes while providing a clear and interpretable measure of change. Land use is measured as the share of district area in each category, reported in percentage points. These three categories do not exhaust all land cover types—other classes such as water bodies, shrubland, or grassland are excluded—so their shares do not sum to 100%.

2.2 Precipitation

The Indian monsoon is part of the larger Asian–Pacific monsoon system, vital to agriculture and the economy. In India, the four monsoon months (June–September) account for about 80% of annual rainfall (Kala, 2019). Evidence suggests that monsoon rainfall—particularly its onset timing and intensity—is affected by global climate phenomena such as El Niño, although these relationships have become more variable in recent decades (Kala, 2019; Kug et al., 2009; Ummenhofer et al., 2011).

I draw precipitation data from NASA's Global Precipitation Measurement (GPM) IMERG project. I use the Integrated Multi-satellitE Retrievals for GPM (IMERG), Version 07B, which is the most recent consolidated release. IMERG is the unified multi-satellite precipitation product of the U.S. GPM mission, designed to provide globally consistent, high-resolution precipitation estimates (Precipitation Processing System (PPS) At NASA GSFC, 2023). These estimates are merged into half-hourly gridded fields at $0.1^\circ \times 0.1^\circ$ spatial resolution (approximately 10×10 km), providing global coverage from June 2000 onwards. This version corrects known satellite biases and ensures consistency with gauge-based climatologies, making it suitable for empirical climate impact studies. Precipitation is expressed in millimeters per hour (mm/hr). Figure 1 illustrates the strong seasonality of Indian rainfall, with monsoon months (June–September) highlighted in red. The series shows substantial interannual variability in monthly rainfall and suggests an upward trend in monsoon intensity over 2001–2010, most pronounced in July–September, which in my sample account on average for 75% of annual precipitation– consistent with Kala (2019).

I follow Kocornik-Mina et al. (2020) and define extreme precipitation events as instances in which monthly rainfall surpasses very high intensity thresholds. In line with their approach, I

construct two indicators: one for whether a district experienced more than 1,000 millimeters of rainfall in at least one month of a given year—a stringent, conservative definition of extreme precipitation—and one for whether it experienced more than 500 millimeters in a month, which I use as a robustness check. Figure 2 maps districts with at least one extreme-precipitation month for three illustrative years—2001 (start of sample), 2005 (mid-sample), and 2010 (end of sample). Dark shading marks districts exceeding the 1,000 mm monthly threshold; lighter shading indicates none. The maps show marked spatial heterogeneity, recurrent clustering in several regions, and year-to-year shifts in location and extent.

2.3 Nightlights

Nightlight data are derived from yearly global satellite data at a spatial resolution of 30 arc-seconds (approximately 1 km at the equator). Nightlights data are obtained from Li et al. (2021), which use temporally calibrated Defense Meteorological Satellite Program (DMSP)-Operational Linescan System (OLS) stable nighttime light (NTL) time series data from 1992–2013 and converted NTL time series from VIIRS (2014–2021). The DMSP and VIIRS data have been harmonised onto the same integer digital number (DN) scale; these values are directly comparable across the full temporal span (1992–2021) and the global spatial domain. Each pixel is encoded as a DN in the range (0, 63), corresponding to the 6-bit quantization of observed brightness. A DN value of 0 indicates no detectable stable lighting, whereas values from 1 to 62 represent increasing brightness.

2.4 Floods

Flood data are drawn from the India Flood Inventory (IFI), a database that consolidates multiple sources on flood events across India (Saharia et al., 2021). Its main component is the Disastrous Weather Events (DWE) publication of the Indian Meteorological Department (IMD), released annually since 1979. The DWE records a wide range of natural hazards, but only flood events were digitized for inclusion in IFI. To expand coverage, IFI integrates two international databases: the Dartmouth Flood Observatory (DFO) and EM-DAT. Whereas EM-DAT and DFO primarily record large, internationally reported disasters, the IMD–DWE contributes more locally documented events. As a result, the IMD–DWE accounts for most observations in IFI (89%, compared with 6% from EM-DAT and 5% from DFO).

The digitization and harmonisation process involved manual and automated verification to produce a geospatially referenced database suitable for research. Nevertheless, several sources

of uncertainty remain. Reporting may be influenced by administrative incentives (e.g., over-reporting when federal assistance depends on reported damages), while under-reporting is possible in remote or less-affected areas. Locational precision also varies, as the original IMD–DWE reports flood locations at the level of districts, states, or regions. Geographic centroids were constructed through the creation of shapefiles for each event, which can introduce bias where the original information lacked granularity.

Despite these limitations, IFI provides the first multi-decadal, georeferenced series of floods for India. Relative to the DFO, which is widely used in the literature (e.g., Kocornik-Mina et al. (2020)) but emphasizes major riverine floods, IFI captures a broader spectrum of events, including smaller pluvial and flash floods that would otherwise go unrecorded. To ensure comparability with prior work, I follow the measurement strategy of Kocornik-Mina et al. (2020), coding a district as flooded in a given year if any part of its territory intersects a recorded event. This broader coverage makes IFI suitable for studying district-level adaptation and land use responses. Figure A1 maps districts with at least one recorded flood in the year, using the India Flood Inventory (IFI). Panels show 2001 (start of sample), 2005 (mid-sample), and 2010 (end of sample). Dark shading marks districts with a flood; lighter shading indicates none. The maps show spatial heterogeneity and regional clustering, with year-to-year shifts in location and extent.

3 Hydrometeorological Framework: From Extreme Precipitation to Flooding

In the Indian monsoon system, large–scale extreme precipitation events arise when low–pressure systems are intensified by secondary cyclonic vortices (Roxy et al., 2017; Chuphal et al., 2025). Warming in the Indian Ocean is associated with more frequent and intense precipitation extremes in central India, despite declines in seasonal totals.

Extreme precipitation may contribute to flooding when storm persistence and spatial coherence interact with antecedent saturation and limited conveyance and drainage capacity. Accordingly, India's floods are predominantly precipitation–driven, but the mapping from "extreme rain" to "flood" is conditional rather than one–to–one.

Conceptually, the following framework explains the two channels through which extreme precipitation affects land use and economic activity: (i) direct rain impacts and (ii) translation into floods via a probabilistic mapping governed by antecedent moisture and routing capacity.

Thus, the main difference–in–differences (DiD) specification identifies the reduced–form effect of extreme precipitation on land use and economic outcomes.

3.1 Extreme Precipitation & Land Use: Double-Damage Channel

For land–use and local activity outcomes, extreme precipitation operates through two distinct channels: (i) a *direct rain–hit* channel (waterlogging, soil erosion, crop/asset damage, urban drainage stress) that can occur without river overbanking; and (ii) a *rain–to–flood* channel, whereby hydrometeorological and infrastructural conditions translate extreme rain into fluvial or pluvial flooding (Roxy et al., 2017; Chuphal et al., 2025).

Two dimensions determine how a rainfall shock translates into damage in district d and year t. First, the *hydrologic state*, S_{dt}, summarizes the remaining capacity of the landscape to absorb water (soils, floodplains, small storages). Second, the *routing context* X_{dt} captures how water is conveyed away (slopes, rivers, drains, urban pipes, levees).

Hydrologic state (S_{dt}): antecedent moisture and storage. S_{dt} summarizes how much rainfall the landscape can still absorb *before* a storm. In practice, this reflects (i) how wet soils and shallow aquifers are and (ii) how full local storages (e.g., ponds, floodplains) remain after recent rain. A higher S_{dt} means less capacity to take in new water, so a larger share of additional rainfall becomes runoff, raising flood likelihood.

Physical and infrastructural context (X_{dt}). The vector X_{dt} summarizes how easily water can be moved off the landscape once it falls. Two elements are most relevant. First, the natural setting and land cover determine how much rain infiltrates versus runs off: gentle slopes and permeable, vegetated surfaces absorb and slow water, while steep terrain and impervious urban areas (roads, roofs) shed it. Second, the capacity of the drainage system—both natural (rivers and floodplains) and built (storm sewers, culverts, retention basins, levees), together with their maintenance and operation—governs how much flow can be carried without overtopping or ponding. When routing and drainage capacity are ample, a given rainfall shock is more likely to be accommodated; when channels are narrow or silted, floodplains constrained, or drainage undersized or poorly maintained, the same shock is more likely to yield local flooding.

Simple conceptual framework. Let $\text{ExtremePrecipitation}_{dt} \in \{0, 1\}$ denote an extreme–rain year in district d and year t, and let $\text{Flood}_{dt} \in \{0, 1\}$ denote a recorded flood. The rain–to–flood

mapping is probabilistic and depends on the state and context:

$$\Pr\big(\text{Flood}_{dt} = 1 \,\big|\, \text{ExtremePrecipitation}_{dt},\, S_{dt},\, X_{dt}\big) \;=\; h\big(\text{ExtremePrecipitation}_{dt},\, S_{dt},\, X_{dt}\big), \tag{1}$$

with $h(\cdot)$ *larger* when an extreme–rain year occurs and when the catchment starts *wetter* (higher S_{dt}). For the context vector X_{dt}, $h(\cdot)$ is *higher* when conveyance and drainage are *constrained* (e.g., narrow or silted channels, high impervious cover, undersized or poorly maintained sewers) and *lower* when routing and storage capacity are *ample* (e.g., vegetated cover, wide floodplains, adequate drains). When S_{dt} is low (dry) and X_{dt} provides good conveyance, much of the shock is absorbed or routed with limited disruption. When S_{dt} is high (wet) or X_{dt} is capacity–constrained, extra rain becomes runoff and water accumulates in fields, streets, and channels.

Economically, this means extreme precipitation can affect outcomes *even without* a formal flood (e.g., waterlogging on farms or urban nuisance flooding) and can also trigger *widespread inundation* once thresholds are exceeded. In general, $0 < \Pr(\text{Flood}_{dt} = 1 \mid \text{ExtremePrecipitation}_{dt} = 1) < 1$: most Indian floods are precipitation–driven, but not every extreme–rain year floods locally, and some floods arise without a local extreme (e.g., upstream inflows or operational releases).

3.2 Empirical implications and mapping to the econometric specification

The framework above implies that extreme precipitation affects outcomes through two distinct but related channels. First, a direct rain–hit component captures damages that arise even in the absence of a recorded flood (e.g., waterlogging, erosion, urban drainage stress). Second, a rain–to–flood component operates when hydrologic state S_{dt} and routing context X_{dt} translate extreme rain into fluvial or pluvial flooding, as summarized by the probabilistic mapping in equation (1). In expectation, both channels contribute to the response of land use and local economic activity to an extreme–rain year.

Let y_{dt} denote a generic district–year outcome. In a static representation, the expected change

in y_{dt} associated with an extreme–precipitation year can be decomposed into

$$\mathbb{E}\big[\Delta y_{dt} \,\big|\, EP_{dt} = 1\big] - \mathbb{E}\big[\Delta y_{dt} \,\big|\, EP_{dt} = 0\big] =$$
$$\beta^{\text{dir}} + \beta^{\text{flood}} \underbrace{\Big(\Pr(Flood_{dt} = 1 \mid EP_{dt} = 1) - \Pr(Flood_{dt} = 1 \mid EP_{dt} = 0) \Big)}_{\pi}.$$

where π is the discrete change in the probability of a recorded flood induced by an extreme–precipitation year. This expression makes clear that the main object of interest is a reduced–form effect of extreme precipitation on land use and economic activity: an extreme–rain year changes outcomes both directly (through β^{dir}) and by increasing the probability of flooding (through $\beta^{\text{flood}}\pi$). In the empirical analysis, I therefore take $\text{ExtremePrecipitation}_{dt}$ as the primary treatment variable and estimate its reduced–form impact on y_{dt} (namely, land use share and economic activity), without attempting to separately identify β^{dir} and β^{flood}.

The empirical strategy in Section 4 operationalizes this framework in three steps. First, equation (2) clarifies how this specification should be interpreted as a *driver–side reduced form*, aggregating the direct rain–hit and rain–to–flood components implied by the framework. Second, the main dynamic design is an event–study (difference–in–differences) specification with distributed lags of extreme–precipitation years (equation (3)), which traces the time profile of the composite response of y_{dt} to an extreme–rain shock. Third, I estimate a separate validation regression (equation (4)) that relates realized floods to extreme–precipitation years, providing quantitative evidence that the precipitation–based treatment captures variation that is relevant for actual flooding and disciplines the probabilistic mapping in equation (1).

4 Empirical Strategy

This section translates the hydrometeorological framework in Section 3 into an econometric design. Consistent with equation (1), I treat extreme–precipitation years as the main exogenous shock and view reported floods as one (imperfect) realization of the rain–to–flood mechanism.

The primary goal is to estimate the dynamic *driver–side reduced form*: how land–use shares and local economic activity (proxied by log night–time lights) respond over time to an extreme–rain year. I proceed in three steps. First, I clarify how the resulting coefficients map into the reduced–form decomposition implied by the framework. Second, I introduce the event–study specification with distributed lags that delivers the main dynamic estimates. Third, I report a separate validation regression that maps extreme–precipitation years into realized floods, which

I interpret as mechanism evidence rather than as a first stage for an instrumental–variables design.

4.1 Interpretation of the reduced form

Let y_{dt} denote the outcome of interest in district d and year t. For land use, y_{dt} is the share of area in cropland, forest, or built–up; coefficients are therefore interpreted in *percentage points*. For local economic activity, y_{dt} is the logarithm of night–time lights; coefficients are in *log points* (approximately percent changes for small magnitudes).

Consistent with the hydrometeorological framework, the reduced form aggregates two economically distinct pathways through which extreme precipitation can affect y_{dt}: a direct rain–hit component and a rain–to–flood component. The expected change in y_{dt} associated with an extreme–rain year can be decomposed as

$$\Delta y_{dt} = \underbrace{\beta^{\text{dir}}\,\text{ExtremePrecipitation}_{dt}}_{\text{direct rain-hit}} + \underbrace{\beta^{\text{flood}}\,\text{Flood}_{dt}}_{\text{rain-to-flood}} + \alpha_d + \lambda_t + \varepsilon_{dt}. \tag{2}$$

Where α_d and λ_t represent respectively district and year fixed effects. In a static specification, the reduced–form coefficient on $\text{ExtremePrecipitation}_{dt}$ corresponds to

$$\beta^{\text{RF}} = \beta^{\text{dir}} + \beta^{\text{flood}}\,\pi,$$

where π is the discrete change in flood probability defined in Section 3. Intuitively, β^{RF} sums the direct impact of excessive rainfall and a flood–mediated component scaled by the change in flood probability induced by an extreme–precipitation year. Estimates based on $\text{ExtremePrecipitation}_{dt}$ therefore identify the *driver–side reduced form*: the aggregate response of outcomes to an extreme–rain year, combining both channels.

District–year aggregation may attenuate short–lived or highly localized impacts, but under the parallel–trends assumption the framework still justifies interpreting the estimated coefficients as average reduced–form effects of precipitation shocks on land use and economic activity. Because the direct rain–hit effect is not constrained to be zero, I do not attempt to separately identify β^{dir} and β^{flood}, nor do I interpret $\text{ExtremePrecipitation}_{dt}$ as a valid instrument for Flood_{dt}. In the main specification, I therefore treat extreme precipitation as the treatment variable and regard reported flood events as potentially endogenous outcomes of the joint influence of S_{dt}, X_{dt}, land use, and adaptation investments. For comparability with the existing

literature, I do estimate specifications that use floods as the treatment in the replication of Kocornik-Mina et al. (2020) in Section 5.4, but those results are interpreted as benchmarks rather than as the primary identification strategy.

4.2 Event-study specification with distributed lags

The main dynamic specification is a standard event–study design around extreme precipitation years. For each district–year, I keep track of whether the district experienced an extreme–precipitation year in the current year or in a number of years before or after.

Formally, let $\text{ExtremePrecipitation}_{d,t-k} = 1$ if district d had at least one month with precipitation above the 1,000 mm threshold in year $t-k$, for $k = 0, 1, \ldots, 5$, and 0 otherwise. Thus $k = 0$ corresponds to the event year itself, $k = 1$ to the first year after an event, and so on up to five years after. These variables are the standard event–time indicators for lags $k = 0, \ldots, 5$.

Because extreme–precipitation years can recur, including in consecutive years, more than one of these indicators can equal one in the same district–year. For example, if a district has extreme–precipitation years in both t and $t-1$, then $\text{ExtremePrecipitation}_{dt} = 1$ and $\text{ExtremePrecipitation}_{d,t-1} = 1$. In that case, the coefficient on each lag measures the marginal contribution of a shock k years earlier, holding constant the pattern of nearby shocks captured by the other lag indicators and the pooled bins.

The main dynamic specification can be written as the following event–study regression at the district–year level:

$$y_{dt} \;=\; \beta_{-2}\,\text{Pooled Lead}_{dt}^{(\leq -2)} + \sum_{k=0}^{5} \beta_k\,\text{ExtremePrecipitation}_{d,t-k} + \beta_{6+}\,\text{Pooled Lag}_{dt}^{(\geq 6)} + \alpha_d + \lambda_t + \varepsilon_{dt}. \quad (3)$$

The unit of observation is a district–year (d, t), and the panel covers all districts from 2001 to 2010. The dependent variable y_{dt} denotes either a land–use share (cropland, forest, or built–up area, in percentage points) or local economic activity (log night–time lights).

The coefficients of primary interest are the event–time coefficients $\{\beta_k\}_{k=0}^{5}$. The omitted category is event time -1, so all coefficients are interpreted relative to the year immediately prior to an extreme–precipitation year. The fixed effects α_d and λ_t absorb, respectively, time–invariant district heterogeneity and common year shocks, while ε_{dt} is an idiosyncratic error term. Standard errors are clustered at the state level. Each β_k is therefore interpreted as the within–district effect of having had an extreme–precipitation year k years earlier, relative to the year immediately before the event and holding all other event–time indicators fixed.

To avoid estimating a long list of very noisy coefficients far from the event, I pool more distant periods into two dummies. The variable Pooled Lead$_{dt}^{(\leq -2)}$ equals one if district d will experience at least one extreme–precipitation year two or more years after t (event times $k \leq -2$), and zero otherwise; its coefficient β_{-2} summarizes average differences in the pooled pre–event years. Symmetrically, Pooled Lag$_{dt}^{(\geq 6)}$ equals one if district d experienced at least one extreme–precipitation year six or more years before t (event times $k \geq 6$); its coefficient β_{6+} captures average longer–run differences in the pooled post–event years. By construction, both pooled variables are maximum values: they record whether there is at least one event in the corresponding window but do not distinguish between one or several shocks.

In event–time terms, let $k = 0$ denote the event year, $k = 1, \ldots, 5$ the first five post–event years, $k = -1$ the year immediately before an event, and $k \leq -2$ and $k \geq 6$ the pooled pre– and post–event bins. Identification comes from comparing the evolution of land use and night-time lights in districts that experience an extreme–precipitation year with the evolution in districts that do not, over horizons from the year of the shock up to five years afterwards. District and year fixed effects absorb permanent differences in geography and common macro shocks, so identification relies on within-district deviations in extreme precipitation over time and on the staggered timing of shocks across districts. For each horizon k, the coefficient β_k measures the average within-district change in outcomes k years after an extreme–precipitation year, relative to the year immediately before the shock, comparing districts that experienced an extreme–precipitation year k years ago to districts that did not at that horizon, conditional on district and year fixed effects. Identification of these dynamic effects relies on a parallel–trends assumption in event time: absent shocks, and conditional on district and year fixed effects, treated and untreated districts would have followed similar trends over the entire pre- and post-event window.

Single–event event–study graph. The main dynamic figure is a standard event–study graph. It plots the estimated coefficients $\{\hat{\beta}_k\}_{k=-2,0,\ldots,5,6+}$ from equation (3), with the pre–event year $k = -1$ normalized to zero and omitted from the regression. Each point on the graph is therefore interpreted as the average within–district change in the outcome y_{dt} k years after an extreme–precipitation year, relative to the year immediately before the event, holding district and year fixed effects and the other event–time indicators fixed. The coefficient on the pooled pre–event bin ($k \leq -2$) is used to discuss pre–trends. Under the parallel–trends assumption, this pre–event coefficient should be close to zero and statistically insignificant. Because overlapping episodes are explicitly modeled through the full vector of event–time indicators and pooled bins, the event–study graph is identified from timing variation in exposure and does

not require "clean" windows with exactly one shock.

Aggregated (compounded) event–study graph. To summarize the cumulative impact of repeated exposure, I also report model–implied paths for $N \in \{2, 3, 4\}$ consecutive annual shocks starting at $t = 0$.[3] These paths are constructed by "stacking" the single–event coefficients: at event time k, the N–shock curve adds the relevant single–event effects that would arise from shocks in each of the prior N years (using the pooled long–lag coefficient for $k \geq 6$). These curves show the predicted cumulative effect of back–to–back extreme–precipitation years under standard assumptions: effects add across years and depend only on the time elapsed since each shock (no interactions or state dependence). In the language of the framework, equation (3) and the associated event–study graphs therefore provide dynamic analogues of the reduced–form effect $\beta^{\text{RF}} = \beta^{\text{dir}} + \beta^{\text{flood}}\pi$, while allowing for multiple episodes of extreme precipitation.

Relation to Modern Difference–in–Differences Methods Because extreme precipitation is a non-absorbing, repeatable, and transitory shock, districts enter and exit treatment multiple times during the sample. This setting does not exhibit staggered adoption of a permanent treatment and therefore does not fall into the standard staggered-adoption case studied by Sun and Abraham (2021) and Callaway and Sant'Anna (2021). The dynamic specification estimated corresponds to a fully-saturated event-time model and coincides algebraically with the unweighted stacked event-study estimator, with the only difference being the implicit equal weighting across event-time observations. This allows me to interpret the impulse–response coefficients directly as an event–study graph, with pre-event coefficients serving as a parallel-trends diagnostic.

4.3 Validation: Extreme Precipitation and realized Floods

Lastly, I verify that the treatment variable, $\text{ExtremePrecipitation}_{dt}$, captures variation that is relevant for realized flooding, as implied by the probabilistic mapping in equation (1). To do so, I estimate a linear probability model with district fixed effects μ_d and year fixed effects τ_t,

$$\text{Flood}_{dt} = \pi \, \text{ExtremePrecipitation}_{dt} + \mu_d + \tau_t + u_{dt}, \tag{4}$$

with standard errors clustered at the state level. Because $\text{ExtremePrecipitation}_{dt}$ is an upstream meteorological driver, while the flood datasets record only a subset of realizations, the

[3] These multi–shock paths are a re–parameterization of the event–study coefficients, not estimates from separate regressions. They are obtained by stacking the single–event impulse responses under a standard linear additivity assumption and do not rely on additional identifying assumptions.

coefficient

$$\pi = \Pr(\text{Flood}_{dt} = 1 \mid \text{ExtremePrecipitation}_{dt} = 1) - \Pr(\text{Flood}_{dt} = 1 \mid \text{ExtremePrecipitation}_{dt} = 0)$$

is expected to be positive but strictly less than one. Hydrometeorologically, not every extreme–rain year generates a flood, and some floods arise without contemporaneous local extremes (e.g., upstream inflows or reservoir releases). Data–source differences in event definition and coverage further attenuate π relative to a one–for–one mapping. Within the conceptual framework, $\hat{\pi}$ therefore provides an empirical counterpart—and likely a lower bound—to the discrete change in flood probability induced by an extreme–precipitation year.

5 Results

5.1 Main results: dynamic effects of extreme precipitation

The main estimates are obtained from the event–study specification in equation (3). This specification traces the evolution of outcomes in districts that experience an extreme–precipitation year relative to their own outcomes in the year immediately prior to exposure, while using districts that are not exposed in the same calendar year as controls. The coefficients can therefore be interpreted as within–district changes in event time relative to the pre–event baseline, averaged over all episodes in the sample and conditional on district and year fixed effects.

Because districts differ in how many pre- and post-event years they contribute, the resulting event-time panel is not balanced. Rather than restricting the sample to balanced event windows, I retain all usable observations and pool more distant periods into two indicators: one for all pre-event years that are at least two years before an extreme-precipitation year, and one for all post-event years that are at least six years after an event. The estimated event-time coefficients $\{\beta_k\}_{k=0}^{5}$ thus trace the dynamic response from the event year through five years afterwards, relative to the year immediately before the event, while β_{-2} and β_{6+} summarize average pre-treatment differences and long-run post-treatment differences in the pooled bins.

Table 2 reports the corresponding regression estimates. Panel A presents the dynamic event–time coefficients, and Panel B reports average post–treatment effects obtained by equal–weighting the first four post–event years. Figures 5–6 display the associated event–study graphs. The last column of Panel A additionally reports the validation regression that maps extreme–precipitation years into IFI–recorded floods, providing a mechanism check for the meteorological treatment.

5.1.1 Dynamic effects

Panel A of Table 2 shows the estimated event–time coefficients from equation (3). For land–use outcomes, exposure to an extreme–precipitation year has no consistent or statistically significant effect on cropland, forest cover, or built–up land in the five years following a shock. Point estimates alternate in sign and remain close to zero in magnitude, indicating the absence of systematic directional responses. For night–time lights, which proxy local economic activity, most coefficients are also indistinguishable from zero. The only exception is a small negative effect at lag 4 (–0.037, significant at the 10% level), which is not corroborated by responses at adjacent lags and is best interpreted as sampling variation rather than evidence of persistent impacts.

The pooled lead coefficient, which summarizes differences two or more years before an event, is close to zero and statistically insignificant for all outcomes. Together with the omission of the $t-1$ period, this standard event–study pattern supports the parallel–trends assumption underlying the difference–in–differences design.

5.1.2 Event–study graphs and compounded responses

Figures 3–6 complement the regression table by displaying the estimated event–study coefficients as impulse–response functions (IRFs). Each figure is divided into two panels. Panel (a) shows a standard event–study graph: the left-hand side plots the single–event coefficients $\{\hat{\beta}_k\}_{k=-2,0,\ldots,5,6+}$ from equation (3), with the pre–event year $k=-1$ normalized to zero and omitted from the regression. The right-hand side of Panel (a) shows model–implied cumulative paths for sequences of two to four consecutive shocks, constructed by linearly combining the single–event coefficients under the assumption of additivity. Panel (b) then breaks down the responses for two, three, and four consecutive events separately, highlighting how repeated exposure would compound the dynamic profile if effects added over time. As described in Section 4, the multi–shock paths are not estimated from separate regressions: they are fitted values implied by the single–event coefficients for hypothetical sequences of $N \in \{2,3,4\}$ back–to–back shocks.

For each outcome, the coefficient on the pooled lead bin (event times $k \leq -2$) lies close to zero and its 95% confidence band includes zero, with no systematic pattern in the pre–event period. For cropland and built–up land, the lead estimates fluctuate mildly but remain statistically indistinguishable from zero; for forest cover and night–time lights, pre–event coefficients are nearly flat. The pre–treatment segments of Panels (a) therefore show no evidence that treated

districts were on different trends than non–treated districts before extreme–precipitation years, consistent with the regression–based pre–trend tests and supporting the parallel–trends assumption.

Across all outcomes, the plots reinforce the message of the regression estimates. For cropland (Figure 3), the point estimates show slight positive deviations in some post–shock years and in the multi–shock scenarios, yet the error bands are wide and the responses are not significant. For forest cover (Figure 4), the point estimates lean negative—consistent with potential losses following repeated shocks—but the confidence intervals include zero throughout. For built–up land (Figure 5), the single–event IRF remains close to zero, with confidence bands covering both modest gains and losses; the compounded paths for multiple shocks suggest small increases in urban share, but these are not statistically distinguishable from zero. For night–time lights (Figure 6), small short–run declines are visible, especially under repeated exposure, but these estimates are imprecise and not statistically different from zero.

Taken together, the event–study graphs show how the distributed–lag specification translates into dynamic adjustment paths. The key finding is that neither isolated shocks nor repeated sequences of shocks lead to systematic, statistically robust shifts in cropland, forest, built–up land, or local economic activity. The visual evidence from the IRFs confirms the regression–based conclusion: extreme–precipitation shocks during the 2000s left no detectable medium–run imprint on land–use patterns or night–time lights.

5.1.3 Average post–treatment effects

To summarize the medium–run impact of extreme–precipitation events more precisely than any single post–event coefficient, I construct an "average post–treatment effect" as a linear combination of the dynamic coefficients in equation (3). Let $\hat{\beta}_k$ denote the estimated coefficients on the contemporaneous and lagged treatment indicators for event times $k = 0, 1, 2, 3$. The summary effect is defined as the equal–weighted average

$$\bar{\beta} \;=\; \frac{1}{4}\sum_{k=0}^{3} \hat{\beta}_k, \tag{5}$$

with standard error obtained from the variance–covariance matrix of $(\hat{\beta}_0, \hat{\beta}_1, \hat{\beta}_2, \hat{\beta}_3)$ using the delta method.

I focus on the 0–3 window because four post–event years is the median horizon available per event in the estimation sample; averaging over this range therefore targets the horizon that

is most consistently observed across districts, improving precision while remaining faithful to the fully dynamic specification. To gauge both statistical and economic significance, I benchmark these average effects against the residual variation in each outcome. For each specification, I compute the standard deviation of the regression residuals, which captures typical year–on–year within–district fluctuations after removing district and year fixed effects and the dynamic impact of extreme–precipitation events. Expressing the half–width of the 95% confidence interval for $\bar{\beta}$ as a fraction of this residual standard deviation shows what share of the remaining unexplained variation could be attributed to systematic medium–run responses to extreme precipitation: small ratios imply that any such systematic responses must be economically small. Conceptually, most of the variation in district–level land–use shares is cross–sectional and slow–moving: some districts are persistently more agricultural or more urban than others, and these level differences are absorbed by the district fixed effects, while common business–cycle and policy shocks are absorbed by the year fixed effects. Once these components and the systematic dynamic response to extreme–precipitation events are netted out, the residual captures only short–run, idiosyncratic fluctuations and measurement noise.

Panel B of Table 2 reports these average post–treatment effects for the baseline definition of an extreme year (monthly rainfall $\geq$ 1000mm) and the corresponding 95% confidence intervals. For cropland, the average effect is -0.020 percentage points with a 95% interval $[-0.071, 0.032]$. The half–width of this interval (0.052 percentage points) is about 0.07 times the residual standard deviation of year-to-year cropland changes (reported in the row "Residual Variation (SD)"), implying that any systematic medium-run cropland response must be smaller than roughly 0.07 residual standard deviations of unexplained fluctuations. Built–up land and night–time lights display a similar pattern: average effects of 0.005 percentage points and 0.003 log points, with confidence-interval half–widths of around 0.07 and 0.12 residual standard deviations, respectively. These estimates exclude even modest systematic shifts in urban expansion or local economic activity. For forest cover, the point estimate is -0.072 percentage points and the 95% interval remains wider, with a half–width of about 0.25 residual standard deviations; here the estimates are still centered near zero but leave room for small effects that cannot be ruled out with comparable precision.

Across cropland, built–up land, and night–time lights, the average effects are close to zero and the 95% confidence intervals cover at most about 0.12 of the residual year–to–year variation in each outcome. In practical terms, any systematic medium–run response along these margins, if present, must be smaller than roughly one–tenth of the fluctuations that remain after controlling for geography and common shocks. Thus, the results document precise null effects

and no detectable spatial reallocation of land or local economic activity in response to extreme precipitation.

5.2 Mechanism evidence: mapping extreme precipitation to floods

Lastly, I validate that the precipitation–based treatment correlates with recorded flood events. Column 5 of Table 2 reports the linear probability model in equation (4), which relates a district–year IFI flood indicator to the extreme–precipitation indicator, controlling for district fixed effects, year fixed effects, and clustering at the state level. The coefficient on the extreme–precipitation indicator is 0.119, statistically significant at the 1% level. Because both variables are dummies and the specification includes fixed effects, this coefficient is interpreted as the within–district change in the conditional probability that IFI records a flood when a year switches from "no extreme precipitation" to "extreme precipitation", holding common year shocks constant. Thus, an extreme–precipitation year is associated with a 12 percentage–point higher probability of an IFI–recorded flood; relative to the mean of the dependent variable in the sample (0.293), this is about a 41% increase.

These results align with the hydrometeorological framework: extreme precipitation is an upstream driver of floods, but the mapping is probabilistic rather than one–to–one. The strong, positive association in the IFI data—while short of determinism—confirms that the precipitation–based treatment captures variation that is relevant for realized flooding in India.

5.3 Robustness: alternative threshold for extreme years

As a robustness check, I repeat the analysis using a looser definition of extreme years based on a 500mm per month threshold, as in Kocornik-Mina et al. (2020). This alternative cutoff classifies more district–years as treated, placing more weight on less intense but more frequent heavy–rain months while leaving the empirical strategy unchanged.

Table 3 summarizes the corresponding regression results. For land–use and night–time lights, Panel A confirms that the dynamic coefficients remain small and unstable in sign across lags, with wide confidence intervals that include zero. Panel B reports the average post–treatment effects, constructed as in Section 5.1.3. For cropland, the average effect is 0.047 with a 95% interval $[-0.026, 0.120]$, implying a confidence–interval half–width of about 0.10 residual standard deviations. Forest cover now exhibits an average effect of -0.038 with bounds $[-0.102, 0.027]$, also corresponding to roughly 0.10 residual standard deviations and tighter than in the baseline specification. For built–up land, the interval half–width is essentially unchanged at about

0.07 residual standard deviations, while for night–time lights it remains around 0.12 residual standard deviations. Lastly, Panel A confirms that the 500mm definition still strongly predicts IFI–recorded floods, consistent with the hydrometeorological mechanism whereby intense monthly rainfall raises flood risk.

Figures A2–A5 present the event–study graphs for the 500mm threshold. These figures are constructed in exactly the same way as Figures 3–6: Panel (a) shows the single–event event–study coefficients and the model–implied cumulative responses to two to four consecutive shocks, and Panel (b) displays the corresponding disaggregated paths. The pre–event segments remain flat and centered around zero for all outcomes, and post–event coefficients are again small and imprecisely estimated. In particular, there is no systematic pattern of persistent gains or losses in cropland, forest cover, built–up area, or night–time lights, even when districts are exposed to repeated years above the 500mm threshold.

Taken together, the baseline and robustness results indicate that, whether extreme years are defined using a 1000mm or 500mm per month cutoff, medium–run effects on cropland, forest cover, built–up area, and local economic activity are small relative to typical year–to–year fluctuations. The data rule out persistent responses larger than roughly one–tenth of the residual interannual variation for most outcomes, reinforcing the conclusion that extreme–precipitation shocks during the 2000s did not trigger systematic reallocation of land use or durable changes in local economic activity at the district level.

5.4 Benchmarking against Kocornik-Mina et al. (2020)

To benchmark the findings against the existing literature, I revisit the India case study in Kocornik-Mina et al. (2020) (henceforth KMMR) and re-estimate their district-level specification using updated data and alternative treatment definitions. KMMR's central analysis asks whether urban economic activity adjusts to major, often recurrent, floods in a global sample. They study the local impact of 53 large urban floods that occurred between 2003 and 2008.

Their study provides a natural point of comparison: while the core analysis is global in scope, covering more than 1,800 cities worldwide, they also conduct a district-level case study for India over the period 2003–2007. The goals of this case study are twofold: (i) to validate night-time lights as a proxy for local economic activity, and (ii) to examine whether large floods affect local economic outcomes as measured by lights and GDP. They first show that night lights and GDP are strongly correlated at the district level, both in cross-section and in panel specifications; for example, in 2003 they estimate an elasticity of 0.44 between log night

lights and log GDP and a reverse elasticity close to one. They then estimate the impact of flooding on night-time lights and GDP using a flood indicator equal to one if any part of a district was flooded in a given year, controlling for district and year fixed effects.

I re-estimate this India specification using the same empirical strategy: a panel of district–year observations with district and year fixed effects and standard errors clustered at the state level. There are two key methodological differences. First, unlike KMMR, I do not restrict the sample to "large floods" (events with at least 100,000 displaced people), but instead use all recorded flood events. This avoids conditioning treatment on outcomes that may themselves be correlated with economic activity. Second, the underlying data sources differ: KMMR use flood events from the DFO, which emphasizes large-scale floods and is less suitable for capturing India's high-frequency, smaller-scale events. For night-time lights, they rely on the DMSP–OLS series, whereas I use the harmonised data of Li et al. (2021), which combine DMSP–OLS and VIIRS.

Additionally, I estimate specifications that use extreme precipitation as the treatment variable. The rationale is that, even without the displacement restriction, flood data may remain endogenous to economic and institutional factors, whereas an extreme–precipitation event is a meteorological shock plausibly orthogonal to local economic conditions. KMMR acknowledge the potential endogeneity of flood data and include extreme precipitation as a robustness check in their global analysis. I instead treat extreme precipitation as a central treatment variable to reduce concerns about selection and strengthen the causal interpretation of the results.

KMMR report small and statistically imprecise coefficients: floods are associated with a -0.020 change in log night–time lights (s.e. 0.014) in the event year and -0.023 (s.e. 0.027) one year later, neither significant at conventional levels. They attribute the limited statistical power to the smaller Indian subsample compared to their global dataset and conclude that "using variation across districts in India alone, we do not have enough power to detect effects of floods on night lights or local GDP."

Table 4 reports the estimates. Column (1) adopts floods as the treatment and finds a statistically significant short–run decline in night–time lights of -0.050 log points, significant at the 1% level. This corresponds to a roughly 5% contraction in local light intensity in the year of the event. The effect is short–lived: Column (2) shows that the lagged coefficient is -0.009, close to zero and insignificant. Columns (3) and (4) use extreme precipitation as the treatment. In Column (3), contemporaneous effects are small and insignificant (-0.016), but a lagged response emerges in Column (4): lights fall by -0.069 log points one year after an

extreme–precipitation event, significant at the 1% level.

These re-estimates are consistent with the central message of the global KMMR analysis: floods depress local economic activity in the short run but do not generate persistent changes. At the same time, they provide sharper evidence for India, both for contemporaneous effects of floods (around 5%) and lagged impacts of extreme precipitation (around 7%). The contrast with KMMR's imprecise India results underscores the importance of treatment definition and sample construction: by avoiding endogenous selection into "large floods" and expanding the effective sample size, the estimates become more precise and easier to interpret.

Taken together with the main results on cropland, forest, and built–up land, this benchmark exercise strengthens the conclusion that extreme precipitation and related hydrological shocks in India during the 2000s generated short–run disruptions in local economic activity but left no systematic medium–run imprint on either land use or night–time lights.

6 Conclusion

Climate change is increasing the frequency and severity of extreme precipitation, raising flood risk and associated economic losses. India is both highly exposed and vulnerable, yet land–use adaptation remains understudied. This paper asks whether exposure to extreme rainfall induces systematic shifts in land allocation and local economic activity across Indian districts.

I assemble an annual district–year panel for 2001–2010 that integrates high–resolution satellite products: extreme–precipitation indicators from NASA's GPM IMERG, land–use shares from the HILDA reconstruction (cropland, forest, built–up), and harmonised night–time lights as a proxy for economic activity. The extreme–precipitation indicator equals one if, in any calendar month of a given year, district rainfall exceeds 1,000 mm. A simple hydrometeorological framework motivates the empirical design by mapping extreme rain to flooding through a probabilistic link governed by antecedent moisture and routing and drainage capacity. Consistent with this framework, I treat extreme precipitation as the main meteorological shock and validate its relevance by showing that an extreme–precipitation year corresponds to an increase of about 41% in district flood occurrence relative to the sample mean.

Using a difference–in–differences event–study design with distributed lags and district and year fixed effects, I find no statistically discernible medium–run changes in cropland, forest cover, or built–up shares following extreme–precipitation shocks. In the average post–treatment window, I can rule out shifts larger than ~ 0.07 s.d. for cropland; for built–up land and night–time

lights, the bounds are ~ 0.07 s.d. and ~ 0.12 s.d., respectively; for forest cover, uncertainty is wider at ~ 0.25 s.d. These standard deviations refer to within–district year–to–year fluctuations after conditioning on district and year fixed effects, so the confidence–interval half–widths for cropland, built–up land, and night–time lights correspond to at most about one–tenth of the residual variation. Results are robust to a looser definition of extreme–precipitation years based on a 500 mm monthly threshold. Model–implied cumulative paths for sequences of repeated shocks likewise show no systematic medium–run response. As a benchmark to the literature, I revisit the India case study in Kocornik-Mina et al. (2020) using richer flood and night–time–light data and alternative treatment definitions. In specifications that mirror their original design, I detect short–run contractions in night–time lights following floods and extreme–precipitation shocks, but—consistent with their global findings—no evidence of persistent losses.

Overall, both isolated and repeated extreme precipitation leave no detectable medium–run imprint on land use or night–time lights. The results suggest that districts do not reallocate land or economic activity in response to climatic extremes; instead, losses are absorbed on existing production structures and settlement patterns. In the hydrometeorological framework, extreme precipitation is an upstream driver that is shaped by global mitigation efforts, whereas the translation into floods depends on modifiable features such as land cover, drainage infrastructure, and the siting of assets in floodplains. The absence of spatial reallocation in the data, combined with rigid land and labor markets, implies that repeated shocks are likely to fall disproportionately on households and firms located in high–risk areas, with the potential to amplify spatial and distributional inequalities.

From a policy perspective, incremental adaptations at the margin are unlikely to be sufficient. Lowering barriers to land reallocation, easing frictions in labor and capital mobility, and enabling more flexible land markets and infrastructure investments may be necessary to improve climate resilience and avoid a rising burden of shocks. Complementary investments in drainage and climate–sensitive infrastructure can alter the mapping from extreme rain to flooding by relaxing local capacity constraints. Without such structural and spatial adjustments, the economic burden of climate shocks is likely to persist or intensify, particularly for the poorest households trapped in high–exposure districts.

References

Amirapu, A., I. Clots-Figueras, and J. P. Rud (2022): "Climate Change and Political Participation: Evidence from India," *SSRN Electronic Journal*.

Barreca, A., K. Clay, O. Deschenes, M. Greenstone, and J. S. Shapiro (2016): "Adapting to Climate Change: The Remarkable Decline in the US Temperature-Mortality Relationship over the Twentieth Century," *Journal of Political Economy*, 124, 105–159, publisher: The University of Chicago Press.

Bazzi, S. (2017): "Wealth Heterogeneity and the Income Elasticity of Migration," *American Economic Journal: Applied Economics*, 9, 219–255.

Blakeslee, D., R. Fishman, and V. Srinivasan (2020): "Way Down in the Hole: Adaptation to Long-Term Water Loss in Rural India," *American Economic Review*, 110, 200–224.

Brooks, W. and K. Donovan (2020): "Eliminating Uncertainty in Market Access: The Impact of New Bridges in Rural Nicaragua," *Econometrica*, 88, 1965–1997, publisher: The Econometric Society.

Burgess, R., O. Deschenes, D. Donaldson, and M. Greenstone (2013): "The Unequal Effects of Weather and Climate Change: Evidence from Mortality in India," .

Burgess, R. and D. Donaldson (2010): "Can Openness Mitigate the Effects of Weather Shocks? Evidence from India's Famine Era," *American Economic Review*, 100, 449–453, publisher: American Economic Association.

Burgess, R. and Donaldson, Dave (2017): "RAilroads and the demise of famine in colonial India," .

Burke, M. and K. Emerick (2016): "Adaptation to Climate Change: Evidence from US Agriculture," *American Economic Journal: Economic Policy*, 8, 106–140.

Burzyński, M., C. Deuster, F. Docquier, and J. de Melo (2022): "Climate Change, Inequality, and Human Migration," *Journal of the European Economic Association*, 20, 1145–1197.

Callaway, B. and P. H. C. Sant'Anna (2021): "Difference-in-Differences with multiple time periods," *Journal of Econometrics*, 225, 200–230.

Carleton, T., A. Jina, M. Delgado, M. Greenstone, T. Houser, S. Hsiang, A. Hultgren, R. E. Kopp, K. E. McCusker, I. Nath, J. Rising, A. Rode, H. K. Seo, A. Viaene, J. Yuan, and A. T. Zhang (2022): "Valuing the Global Mortality Consequences of Climate Change Accounting for Adaptation Costs and Benefits*," *The Quarterly Journal of Economics*, 137, 2037–2105.

Cattaneo, C. and G. Peri (2016): "The migration response to increasing temperatures," *Journal of Development Economics*, 122, 127–146.

Chen, G. (2024): "How stronger land systems can spur economic growth and jobs," .

Chuphal, D. S., I. Malik, R. Singh, G. Vangala, M. Niranjannaik, U. Vegad, N. Dilip K, P. Mukhopadhyay, J. P. Selvan, V. Kapadia, and V. Mishra (2025): "Multi-Day Extreme Precipitation Caused Major Floods in India During Summer Monsoon of 2024," *Earth's Future*, 13, e2024EF005497, _eprint: https://agupubs.onlinelibrary.wiley.com/doi/pdf/10.1029/2024EF005497.

Colmer, J. (2021): "Temperature, Labor Reallocation, and Industrial Production: Evidence from India," *American Economic Journal: Applied Economics*, 13, 101–124.

Costinot, A., D. Donaldson, and C. Smith (2016): "Evolving Comparative Advantage and the Impact of Climate Change in Agricultural Markets: Evidence from 1.7 Million Fields around the World," *Journal of Political Economy*, 124, 205–248, publisher: The University of Chicago Press.

Dar, M. H., A. de Janvry, K. Emerick, D. Raitzer, and E. Sadoulet (2013): "Flood-tolerant rice reduces yield variability and raises expected yield, differentially benefitting socially disadvantaged groups," *Scientific Reports*, 3, 3315.

Das, M., A. Das, and P. Pereira (2024): "Impact of urbanization induced land use and land cover change on ecological space quality- mapping and assessment in Delhi (India)," *Urban Climate*, 53, 101818.

Dell, M., B. F. Jones, and B. A. Olken (2012): "Temperature Shocks and Economic Growth: Evidence from the Last Half Century," *American Economic Journal: Macroeconomics*, 4, 66–95, publisher: American Economic Association.

——— (2014): "What Do We Learn from the Weather? The New Climate-Economy Literature," *Journal of Economic Literature*, 52, 740–798, publisher: American Economic Association.

Deschênes, O. and M. Greenstone (2007): "The Economic Impacts of Climate Change: Evidence from Agricultural Output and Random Fluctuations in Weather," *American Economic Review*, 97, 354–385, publisher: American Economic Association.

——— (2011): "Climate Change, Mortality, and Adaptation: Evidence from Annual Fluctuations in Weather in the US," *American Economic Journal: Applied Economics*, 3, 152–185, publisher: American Economic Association.

Emerick, K. (2018): "Agricultural productivity and the sectoral reallocation of labor in rural India," *Journal of Development Economics*, 135, 488–503.

FAO (2000): "LAND COVER CLASSIFICATION SYSTEM," .

Ghosh, S., D. Das, S.-C. Kao, and A. R. Ganguly (2012): "Lack of uniform trends but increasing spatial variability in observed Indian rainfall extremes," *Nature Climate Change*, 2, 86–91, publisher: Nature Publishing Group.

Grosset-Touba, F., A. Papp, and C. Taylor (2024): "Rain follows the forest: Land use policy, climate change, and adaptation," .

Guiteras, R. (2009): "The Impact of Climate Change on Indian Agriculture," .

Henderson, J. V., A. Storeygard, and U. Deichmann (2017): "Has climate change driven urbanization in Africa?" *Journal of Development Economics*, 124, 60–82.

Hornbeck, R. and P. Keskin (2014): "The Historically Evolving Impact of the Ogallala Aquifer: Agricultural Adaptation to Groundwater and Drought," *American Economic Journal: Applied Economics*, 6, 190–219.

Hsiao, A. (2025): "Sea Level Rise and Urban Adaptation," .

Hultgren, A., T. Carleton, M. Delgado, D. R. Gergel, M. Greenstone, T. Houser, S. Hsiang, A. Jina, R. E. Kopp, S. B. Malevich, K. E. McCusker, T. Mayer, I. Nath, J. Rising, A. Rode, and J. Yuan (2025): "Impacts of climate change on global agriculture accounting for adaptation," *Nature*, 642, 644–652, publisher: Nature Publishing Group.

Intergovernmental Panel on Climate Change (IPCC) (2022): "Land–climate interactions," in *Climate Change and Land: an IPCC special report on climate change, desertification, land degradation, sustainable land management, food security, and greenhouse gas fluxes in terrestrial ecosystems.*, Cambridge: Cambridge University Press.

Intergovernmental Panel On Climate Change (IPCC) (2023): *Climate Change 2021 – The Physical Science Basis: Working Group I Contribution to the Sixth Assessment Report of the Intergovernmental Panel on Climate Change*, Cambridge University Press, 1 ed.

Kala, N. (2019): "LEARNING, ADAPTATION, AND CLIMATE UNCERTAINTY: EVIDENCE FROM INDIAN AGRICULTURE," .

Khanna, G., W. Liang, A. M. Mobarak, and R. Song (2025): "The Productivity Consequences of Pollution-Induced Migration in China," *American Economic Journal: Applied Economics*, 17, 184–224.

Kocornik-Mina, A., T. K. J. McDermott, G. Michaels, and F. Rauch (2020): "Flooded Cities," *American Economic Journal: Applied Economics*, 12, 35–66.

Kug, J.-S., F.-F. Jin, and S.-I. An (2009): "Two Types of El Niño Events: Cold Tongue El Niño and Warm Pool El Niño," *Journal of Climate*, 22, 1499–1515.

Lehmann, J., D. Coumou, and K. Frieler (2015): "Increased record-breaking precipitation events under global warming," *Climatic Change*, 132, 501–515.

Li, X., Y. Zhou, M. Hejazi, M. Wise, C. Vernon, G. Iyer, and W. Chen (2021): "Global urban growth between 1870 and 2100 from integrated high resolution mapped data and urban dynamic modeling," *Communications Earth & Environment*, 2, 1–10, publisher: Nature Publishing Group.

Liu, M., Y. Shamdasani, and V. Taraz (2023): "Climate Change and Labor Reallocation: Evidence from Six Decades of the Indian Census," *American Economic Journal: Economic Policy*, 15, 395–423.

Moscona, J. and K. A. Sastry (2023): "Does Directed Innovation Mitigate Climate Damage? Evidence from U.S. Agriculture*," *The Quarterly Journal of Economics*, 138, 637–701.

Moulds, S., W. Buytaert, and A. Mijic (2018): "A spatio-temporal land use and land cover reconstruction for India from 1960–2010," *Scientific Data*, 5, 180159, publisher: Nature Publishing Group.

Pelli, M., J. Tschopp, N. Bezmaternykh, and K. M. Eklou (2023): "In the eye of the storm: Firms and capital destruction in India," *Journal of Urban Economics*, 134, publisher: Elsevier.

Precipitation Processing System (PPS) At NASA GSFC (2023): "GPM IMERG Final Precipitation L3 1 month 0.1 degree x 0.1 degree V07," .

Raghuvanshi, A. S., R. M. Trigo, and A. Agarwal (2025): "Climatology of extreme precipitation spells induced by cloudburst-like events during the Indian Summer Monsoon," *Journal of Hydrology X*, 26, 100197.

Rexer, J. and S. Sharma (2024): *Climate Change Adaptation: What Does the Evidence Say ?*, Washington, DC: World Bank.

Roxy, M. K., S. Ghosh, A. Pathak, R. Athulya, M. Mujumdar, R. Murtugudde, P. Terray, and M. Rajeevan (2017): "A threefold rise in widespread extreme rain events over central India," *Nature Communications*, 8, 708, publisher: Nature Publishing Group.

Saharia, M., A. Jain, R. R. Baishya, S. Haobam, O. P. Sreejith, D. S. Pai, and A. Rafieeinasab (2021): "India flood inventory: creation of a multi-source national geospatial database to facilitate comprehensive flood research," *Natural Hazards*, 108, 619–633.

Somanathan, E., R. Somanathan, A. Sudarshan, and M. Tewari (2021): "The Impact of Temperature on Productivity and Labor Supply: Evidence from Indian Manufacturing," *Journal of Political Economy*, 129, 1797–1827, publisher: University of Chicago Press.

Sun, L. and S. Abraham (2021): "Estimating dynamic treatment effects in event studies with heterogeneous treatment effects," *Journal of Econometrics*, 225, 175–199.

Taraz, V. (2017): "Adaptation to climate change: historical evidence from the Indian monsoon," *Environment and Development Economics*, 22, 517–545.

Tellman, B., J. A. Sullivan, C. Kuhn, A. J. Kettner, C. S. Doyle, G. R. Brakenridge, T. A. Erickson, and D. A. Slayback (2021): "Satellite imaging reveals increased proportion of population exposed to floods," *Nature*, 596, 80–86, publisher: Nature Publishing Group.

Tian, H., K. Banger, T. Bo, and V. K. Dadhwal (2014): "History of land use in India during 1880–2010: Large-scale land transformations reconstructed from satellite data and historical archives," *Global and Planetary Change*, 121, 78–88.

Torhonen, M.-P. (2024): "Securing Land Tenure to Secure a Sustainable Future," .

Ummenhofer, C. C., A. Sen Gupta, Y. Li, A. S. Taschetto, and M. H. England (2011): "Multi-decadal modulation of the El Niño–Indian monsoon relationship by Indian Ocean variability," *Environmental Research Letters*, 6, 034006.

7 Figures

Figure 1: Monthly Average Precipitation (mm/hr)

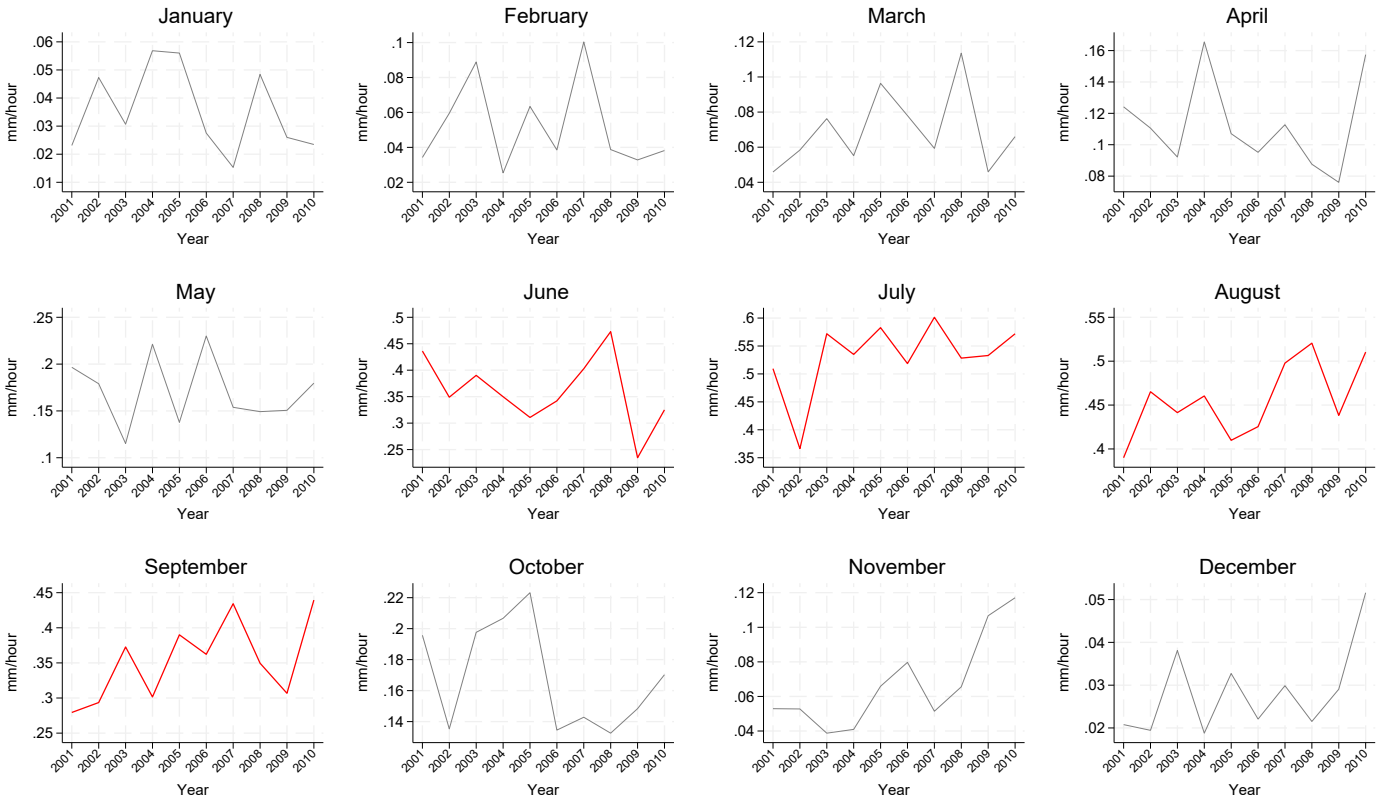

Notes: Each panel plots the national monthly average precipitation for the period 2001–2010, expressed in millimeters per hour. Panels correspond to calendar months from January to December. The series highlights the strong seasonality of rainfall in India, with the monsoon months (June to September) marked in red. See Section 2 for a full description of the data sources.

Figure 2: Maps of Extreme Precipitation events

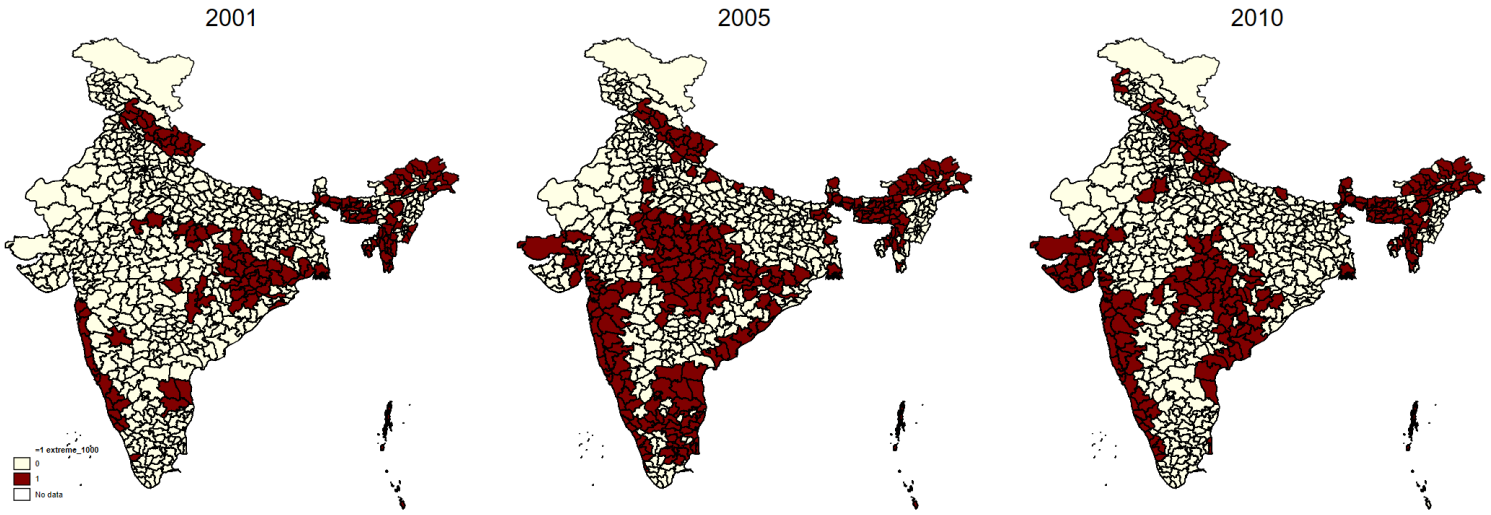

Notes: The maps display the spatial distribution of extreme precipitation across districts for three illustrative years: 2001 (beginning of sample), 2005 (mid-sample), and 2010 (end of sample). Dark shading indicates districts that experienced at least one extreme precipitation event in the corresponding year, while lighter shading denotes districts without such events. An extreme precipitation event is defined as any month in which a district recorded more than 1000 millimeters of rainfall. See Section 2 for a full description of the data sources.

Figure 3: Event-studies - Percentage Share of Cropland

(a) Main plots

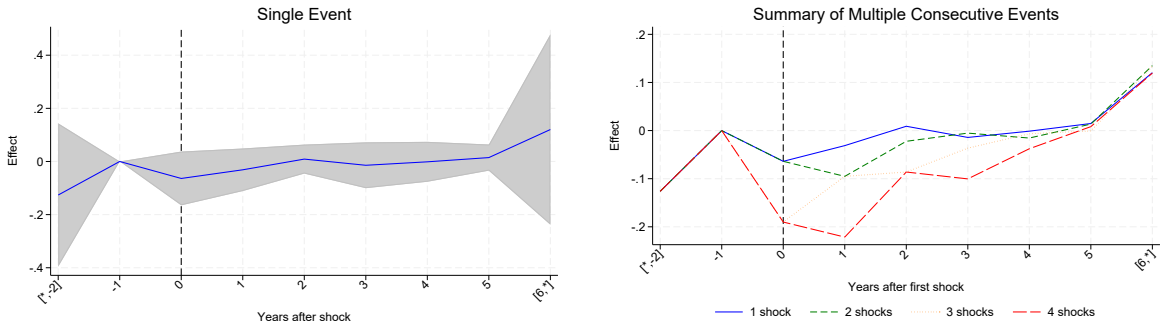

(b) Breakdown by Number of Consecutive Events

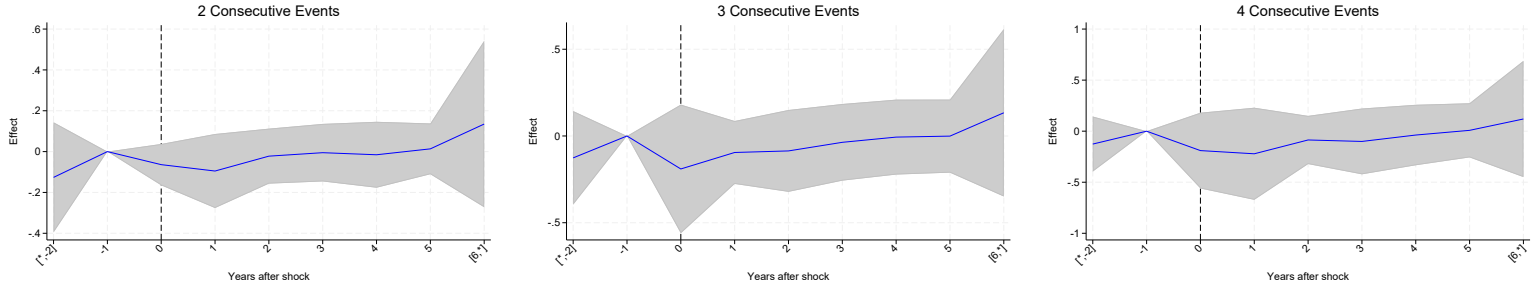

Notes: This figure reports event–study estimates of the dynamic response of Percentage Share of Cropland to extreme–precipitation years defined using a 1000mm per month threshold. All coefficients come from the event–study specification in equation (3), with district and year fixed effects and standard errors clustered at the state level. The vertical dashed line marks event time zero (the year of an extreme–precipitation year); the solid blue line traces point estimates and the shaded gray band represents 95% confidence intervals. Panel (a) shows, on the left, the single–event event–study profile, and, on the right, the model–implied cumulative responses for sequences of two to four consecutive extreme–precipitation years, obtained by linearly combining the single–event coefficients under the assumption of additivity. Panel (b) disaggregates these cumulative paths by plotting separate event–study graphs for districts experiencing exactly two, three, or four consecutive shocks. See Section 2 for a full description of the data sources and Section 5 for a full discussion of the results.

Figure 4: Event-studies - Percentage Share of Forest

(a) Main plots

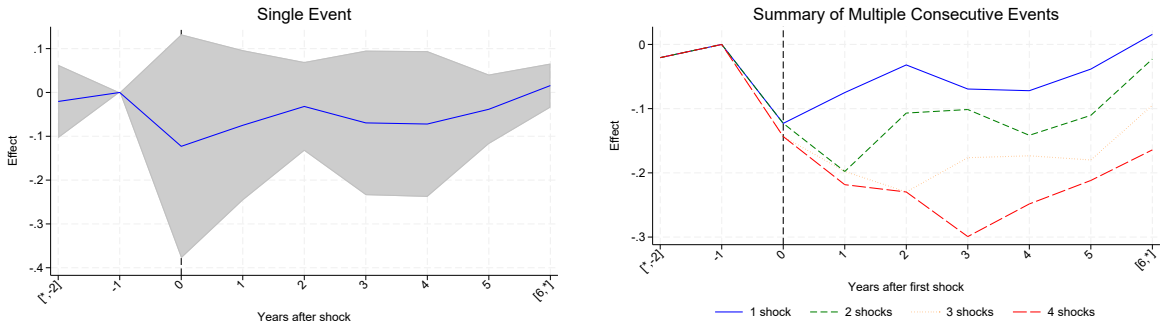

(b) Breakdown by Number of Consecutive Events

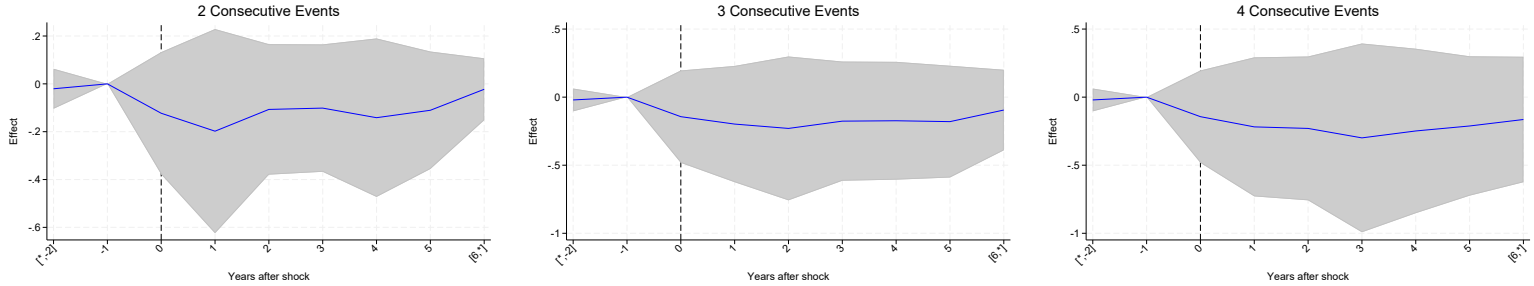

Notes: This figure reports event–study estimates of the dynamic response of Percentage Share of Forest to extreme–precipitation years defined using a 1000mm per month threshold. All coefficients come from the event–study specification in equation (3), with district and year fixed effects and standard errors clustered at the state level. The vertical dashed line marks event time zero (the year of an extreme–precipitation year); the solid blue line traces point estimates and the shaded gray band represents 95% confidence intervals. Panel (a) shows, on the left, the single–event event–study profile, and, on the right, the model–implied cumulative responses for sequences of two to four consecutive extreme–precipitation years, obtained by linearly combining the single–event coefficients under the assumption of additivity. Panel (b) disaggregates these cumulative paths by plotting separate event–study graphs for districts experiencing exactly two, three, or four consecutive shocks. See Section 2 for a full description of the data sources and Section 5 for a full discussion of the results.

Figure 5: Event-studies - Percentage Share of Build-Up

(a) Main plots

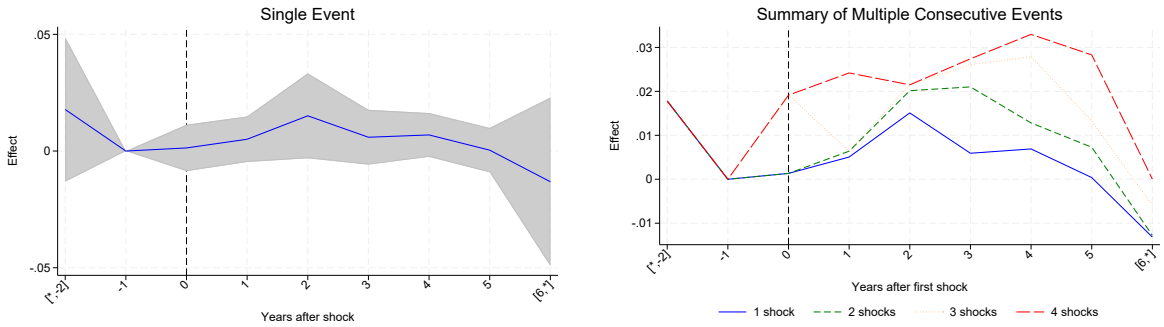

(b) Breakdown by Number of Consecutive Events

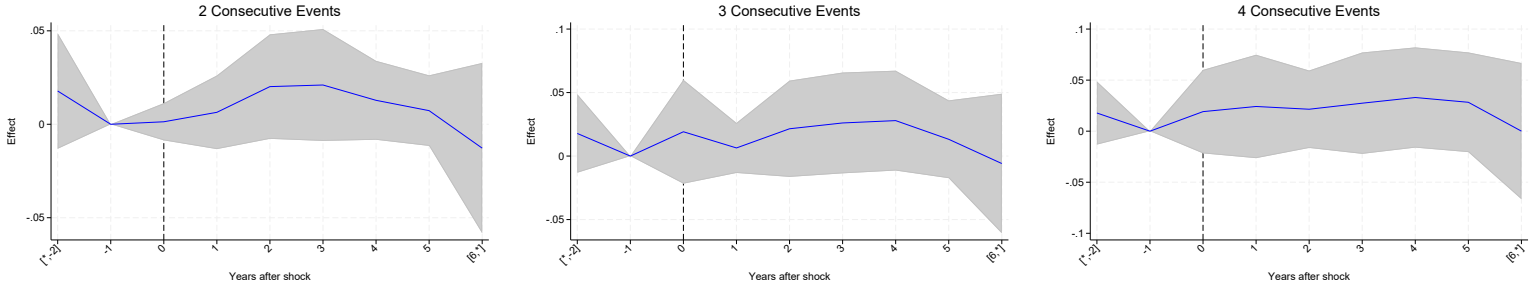

Notes: This figure reports event–study estimates of the dynamic response of Percentage Share of Build-Up to extreme–precipitation years defined using a 1000mm per month threshold. All coefficients come from the event–study specification in equation (3), with district and year fixed effects and standard errors clustered at the state level. The vertical dashed line marks event time zero (the year of an extreme–precipitation year); the solid blue line traces point estimates and the shaded gray band represents 95% confidence intervals. Panel (a) shows, on the left, the single–event event–study profile, and, on the right, the model–implied cumulative responses for sequences of two to four consecutive extreme–precipitation years, obtained by linearly combining the single–event coefficients under the assumption of additivity. Panel (b) disaggregates these cumulative paths by plotting separate event–study graphs for districts experiencing exactly two, three, or four consecutive shocks. See Section 2 for a full description of the data sources and Section 5 for a full discussion of the results.

Figure 6: Event-studies - Ln Nighlight

(a) Main plots

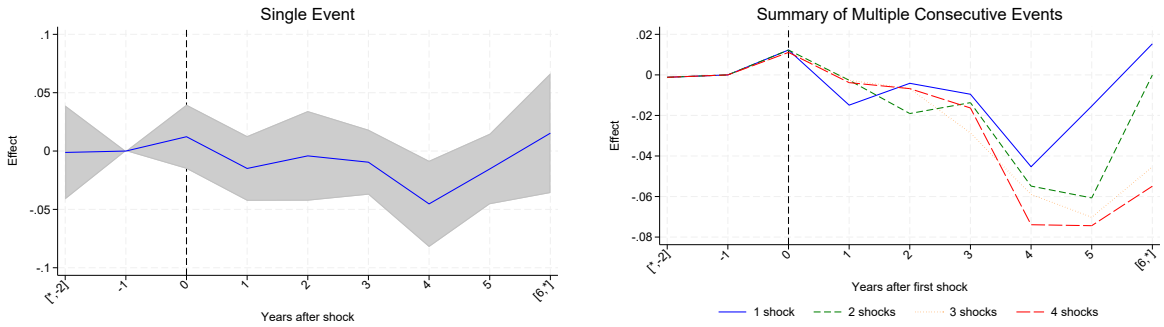

(b) Breakdown by Number of Consecutive Events

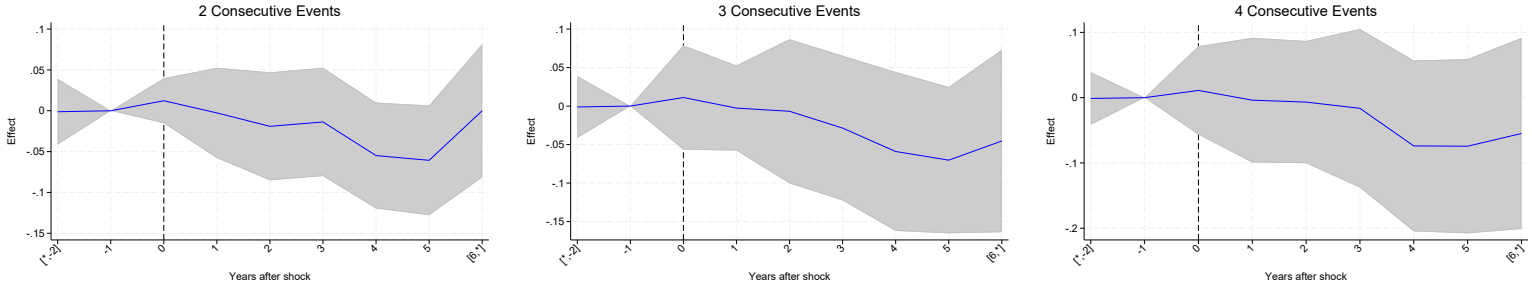

Notes: This figure reports event–study estimates of the dynamic response of Ln Nighlight to extreme–precipitation years defined using a 1000mm per month threshold. All coefficients come from the event–study specification in equation (3), with district and year fixed effects and standard errors clustered at the state level. The vertical dashed line marks event time zero (the year of an extreme–precipitation year); the solid blue line traces point estimates and the shaded gray band represents 95% confidence intervals. Panel (a) shows, on the left, the single–event event–study profile, and, on the right, the model–implied cumulative responses for sequences of two to four consecutive extreme–precipitation years, obtained by linearly combining the single–event coefficients under the assumption of additivity. Panel (b) disaggregates these cumulative paths by plotting separate event–study graphs for districts experiencing exactly two, three, or four consecutive shocks. See Section 2 for a full description of the data sources and Section 5 for a full discussion of the results.

8 Tables

Table 1: Summary Statistics

	N. Observations	Mean	SD	Min	Max
Percentage Share Cropland	7420	59.338	29.271	0.000	98.303
Percentage Share Forest	7420	24.390	26.615	0.000	100.000
Percentage Share Build-Up	7420	3.750	11.677	0.000	98.583
Ln Nighlight	7224	0.933	1.576	-6.821	4.127
= 1 Extreme Precipitation	7260	0.269	0.444	0.000	1.000
= 1 Flood	7420	0.287	0.452	0.000	1.000

Notes: This Table reports the summary statistics for the main set of variables employed in the analysis. See Section 2 for a description of the variables and sources.

Table 2: Main Table

	Land Use (percentage shares)			Ln Nighlight	Mechanism
	(1)	(2)	(3)	(4)	(5)
	Cropland	Forest	Built-up	Light	=1 Flood
Pooled Lead	-0.126	-0.021	0.018	-0.001	
	[0.138]	[0.043]	[0.016]	[0.021]	
= 1 Extreme Precipitation	-0.064	-0.123	0.001	0.012	0.119***
	[0.052]	[0.130]	[0.005]	[0.014]	[0.032]
=1 Lag 1 Extreme Precipitation	-0.031	-0.075	0.005	-0.015	
	[0.041]	[0.087]	[0.005]	[0.014]	
=1 Lag 2 Extreme Precipitation	0.009	-0.032	0.015	-0.004	
	[0.028]	[0.052]	[0.009]	[0.020]	
=1 Lag 3 Extreme Precipitation	-0.014	-0.069	0.006	-0.010	
	[0.044]	[0.084]	[0.006]	[0.014]	
=1 Lag 4 Extreme Precipitation	-0.001	-0.072	0.007	-0.045**	
	[0.038]	[0.085]	[0.005]	[0.019]	
=1 Lag 5 Extreme Precipitation	0.015	-0.038	0.000	-0.015	
	[0.025]	[0.040]	[0.005]	[0.015]	
Pooled Lag	0.120	0.016	-0.013	0.015	
	[0.183]	[0.026]	[0.018]	[0.026]	
Mean dep. var.	60.210	24.088	3.434	0.963	0.293
Observations	4356	4356	4356	4292	7260
States	35	35	35	35	35
Panel B: Average post treatment effect					
Residual Variation (SD)	0.763	0.658	0.217	0.245	
Average post treatment effect (Years 0–3)	-0.020	-0.072	0.005	0.003	
95% CI lower bound	-0.071	-0.237	-0.009	-0.026	
95% CI upper bound	0.032	0.094	0.019	0.032	

Notes: This table reports the main event–study estimates. Panel A presents the dynamic event–time coefficients from the baseline specification in equation (3) for the four main outcomes (cropland, forest, built–up area, and log night–time lights). Panel B aggregates these dynamic coefficients over the 0–3 year window, corresponding to the median post–event horizon in the sample; for each outcome, it reports the average post–treatment effect, the residual standard deviation of the outcome, and 95% confidence intervals. The last column of Panel A (Column 5) reports the validation regression that links extreme–precipitation years to IFI–recorded floods, estimated using the linear probability model in equation (4). All regressions include district and year fixed effects. Standard errors in brackets: clustered at state level. Stars indicate significance in the usual way. See Section 2 for a full description of the data sources and Section 5 for a full discussion of the results.

Table 3: Robustness: 500 mm/month

	Land Use (percentage shares)			Ln Nighlight	Mechanism
	(1)	(2)	(3)	(4)	(5)
	Cropland	Forest	Built-up	Light	=1 Flood
Pooled Lead - 500mm	-0.482	-0.007	0.034	0.055	
	[0.412]	[0.024]	[0.042]	[0.041]	
= 1 Extreme Month - 500mm	-0.050	-0.080*	-0.009	-0.004	0.106***
	[0.030]	[0.045]	[0.009]	[0.023]	[0.035]
=1 Lag 1 Extreme Month - 500mm	0.003	-0.046	-0.024***	0.057**	
	[0.025]	[0.047]	[0.008]	[0.024]	
=1 Lag 2 Extreme Month - 500mm	0.081	-0.038	-0.007	0.021	
	[0.071]	[0.039]	[0.011]	[0.022]	
=1 Lag 3 Extreme Month - 500mm	0.153*	0.013	-0.009	0.010	
	[0.087]	[0.031]	[0.012]	[0.024]	
=1 Lag 4 Extreme Month - 500mm	0.099*	-0.023	0.005	-0.015	
	[0.051]	[0.017]	[0.013]	[0.023]	
=1 Lag 5 Extreme Month - 500mm	0.087**	0.024	0.010	0.008	
	[0.035]	[0.019]	[0.010]	[0.017]	
Pooled Lag - 500mm	0.000	0.000	0.000	0.000	
	[.]	[.]	[.]	[.]	
Mean dep. var.	60.210	24.088	3.434	0.963	0.293
Observations	4356	4356	4356	4292	7260
States	35	35	35	35	35
Panel B: Average post treatment effect					
Residual Variation (SD)	0.763	0.658	0.217	0.245	
Average post treatment effect (Years 0–3)	0.047	-0.038	-0.012	0.021	
95% CI lower bound	-0.026	-0.102	-0.026	-0.009	
95% CI upper bound	0.120	0.027	0.002	0.051	

Notes: This table reports robustness checks using an alternative definition of extreme years based on a 500mm per month threshold. Panel A presents the dynamic event–time coefficients from the event–study specification in equation (3), re–estimated with the 500mm extreme–precipitation indicator. Panel B reports the corresponding average post–treatment effects over the 0–3 year window, constructed as in Section 5.1.3. As in Table 2, the last column of Panel A reports the validation regression of IFI–recorded floods on the extreme–precipitation indicator (equation (4)), now using the 500mm threshold. All regressions include district and year fixed effects. Standard errors in brackets: clustered at state level. Stars indicate significance in the usual way. See Section 2 for a full description of the data sources and Section 5 for a full discussion of the results.

Table 4: India benchmark estimates following Kocornik-Mina et al. (2020)

	Flood treatment indicator		Extreme–precipitation indicator	
	(1)	(2)	(3)	(4)
	Ln Nightlight	Ln Nightlight	Ln Nightlight	Ln Nightlight
=1 Flood	-0.050***			
	[0.012]			
=1 Lag 1 Flood		-0.009		
		[0.014]		
=1 Extreme Precipitation			-0.016	
			[0.021]	
=1 Lag 1 Extreme Precipitation				-0.069***
				[0.022]
District FEs	Yes	Yes	Yes	Yes
Year FEs (2003-07)	Yes	Yes	Yes	Yes
Mean dep. var.	1.000	1.000	1.000	1.000
Observations	3609	3609	3571	3571

Notes: This table reports district–level estimates for India from a specification that follows Kocornik-Mina et al. (2020) (KMMR). Columns (1)–(2) use a flood treatment indicator equal to one if any part of a district intersects a recorded flood in year t (column 1) or year $t-1$ (column 2). Columns (3)–(4) replace this with an extreme–precipitation indicator equal to one if monthly rainfall exceeds 1,000 mm in any month of year t (column 3) or year $t-1$ (column 4). All regressions include district and year fixed effects. Standard errors, in brackets, are clustered at the state level; Stars indicate significance in the usual way. Relative to KMMR, the estimates use all recorded floods rather than only "large" floods, rely on the India Flood Inventory (IFI) rather than DFO, and use harmonised night–time lights from Li et al. (2021). See Section 2 for a full description of the data sources. See Section 5.4 for further discussion.

A Appendix

Figure A1: Maps Floods Events

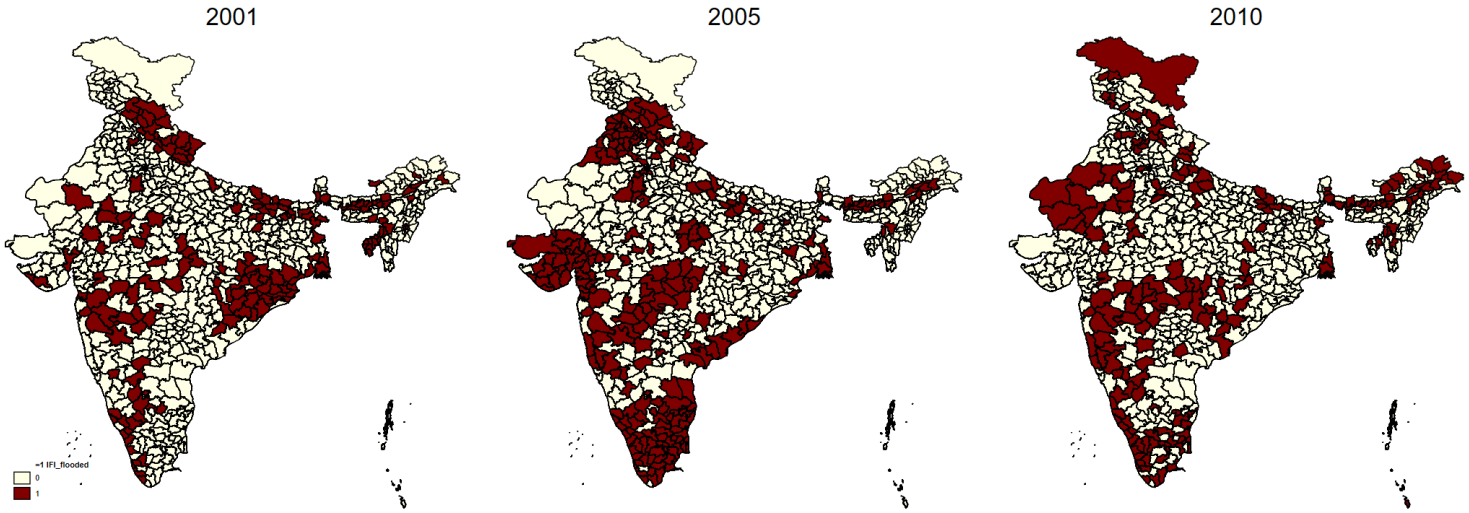

Notes: The maps display the spatial distribution of floods across districts for three illustrative years: 2001 (beginning of sample), 2005 (mid-sample), and 2010 (end of sample). Dark shading indicates districts that experienced at least one flood event in the corresponding year, while lighter shading denotes districts without such events. See Section 2 for a full description of the data sources.

Figure A2: Robustness: Event-Studies (500 mm/month) - Percentage Share of Cropland

(a) Main plots

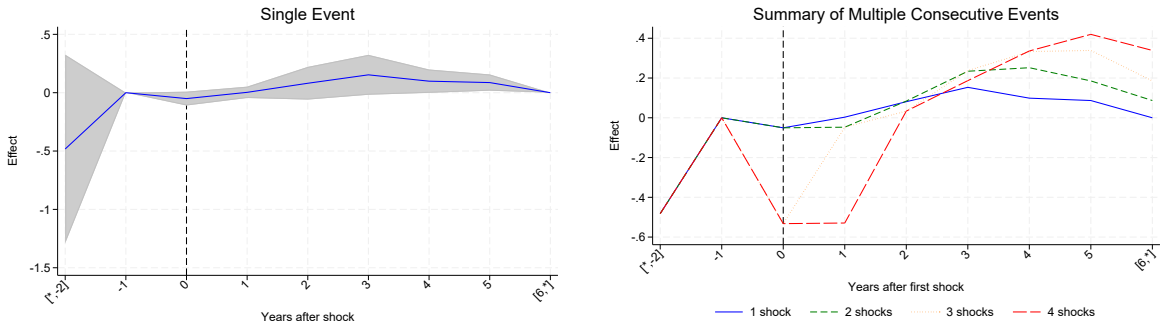

(b) Breakdown by Number of Consecutive Events

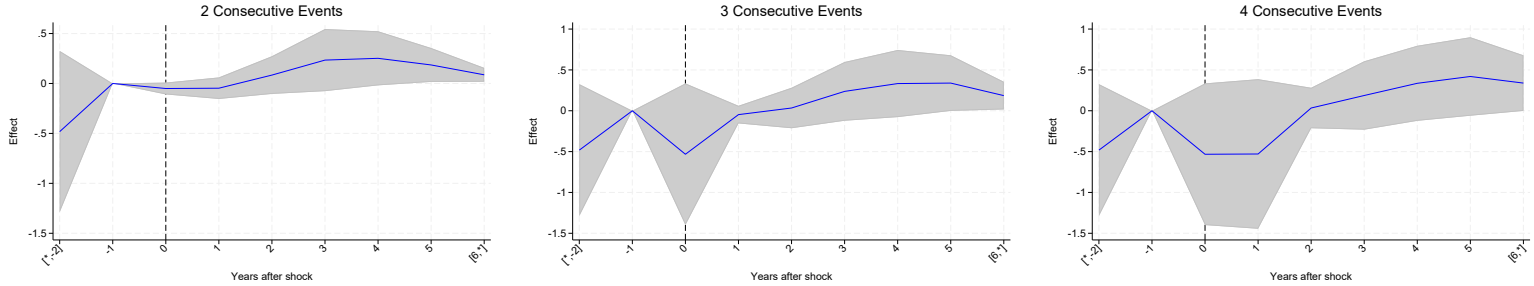

Notes: This figure reports event–study estimates of the dynamic response of Percentage Share of Cropland to extreme–precipitation years defined using a 500mm per month threshold. All coefficients come from the event–study specification in equation (3), with district and year fixed effects and standard errors clustered at the state level. The vertical dashed line marks event time zero (the year of an extreme–precipitation year, $t = 0$); the solid blue line traces point estimates and the shaded gray band represents 95% confidence intervals. Panel (a) shows, on the left, the single–event event–study profile, and, on the right, the model–implied cumulative responses for sequences of two to four consecutive extreme–precipitation years, obtained by linearly combining the single–event coefficients under the assumption of additivity. Panel (b) disaggregates these cumulative paths by plotting separate event–study graphs for districts experiencing exactly two, three, or four consecutive shocks. See Section 2 for a full description of the data sources and Section 5 for a full discussion of the results.

Figure A3: Robustness: Event-Studies (500 mm/month) - Percentage Share of Forest

(a) Main plots

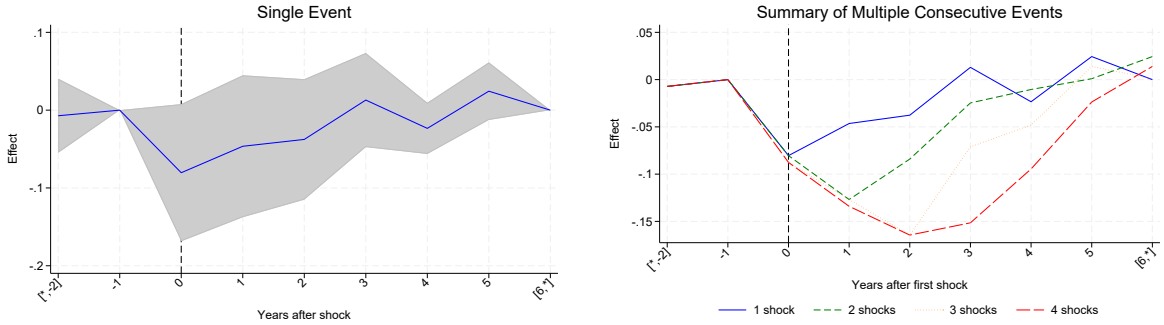

(b) Breakdown by Number of Consecutive Events

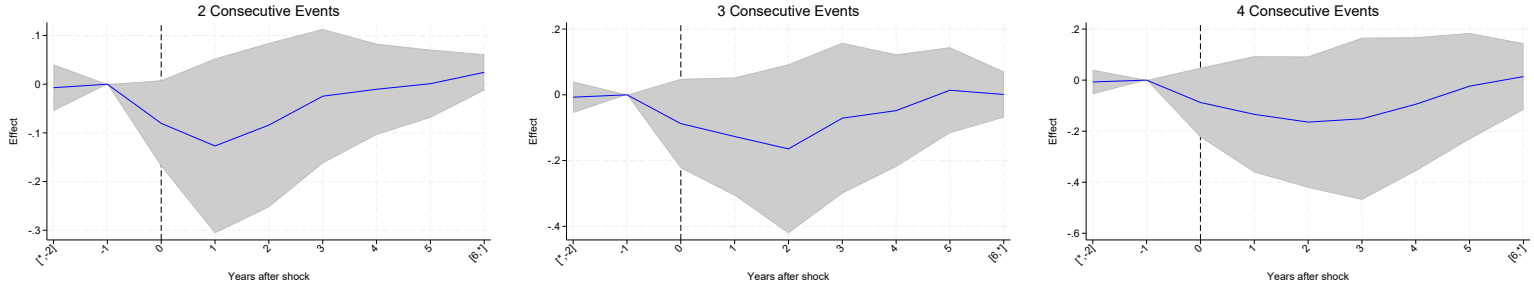

Notes: This figure reports event–study estimates of the dynamic response of Percentage Share of Forest to extreme–precipitation years defined using a 500mm per month threshold. All coefficients come from the event–study specification in equation (3), with district and year fixed effects and standard errors clustered at the state level. The vertical dashed line marks event time zero (the year of an extreme–precipitation year, $t = 0$); the solid blue line traces point estimates and the shaded gray band represents 95% confidence intervals. Panel (a) shows, on the left, the single–event event–study profile, and, on the right, the model–implied cumulative responses for sequences of two to four consecutive extreme–precipitation years, obtained by linearly combining the single–event coefficients under the assumption of additivity. Panel (b) disaggregates these cumulative paths by plotting separate event–study graphs for districts experiencing exactly two, three, or four consecutive shocks. See Section 2 for a full description of the data sources and Section 5 for a full discussion of the results.

Figure A4: Robustness: Event-Studies (500 mm/month) - Percentage Share of Build-Up

(a) Main plots

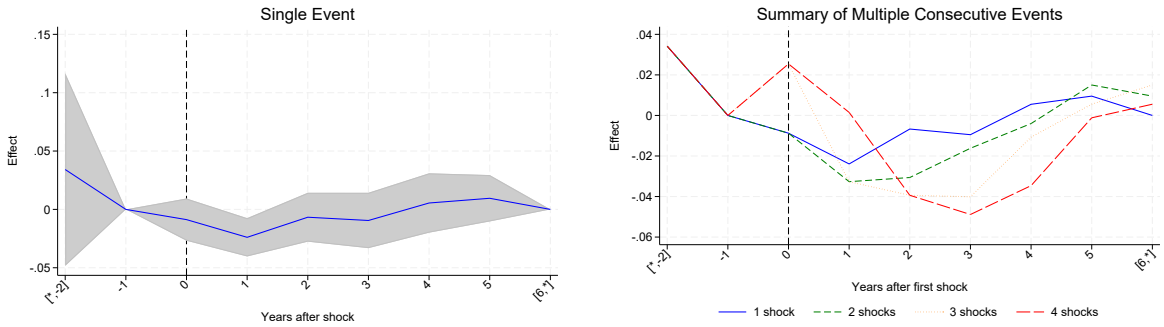

(b) Breakdown by Number of Consecutive Events

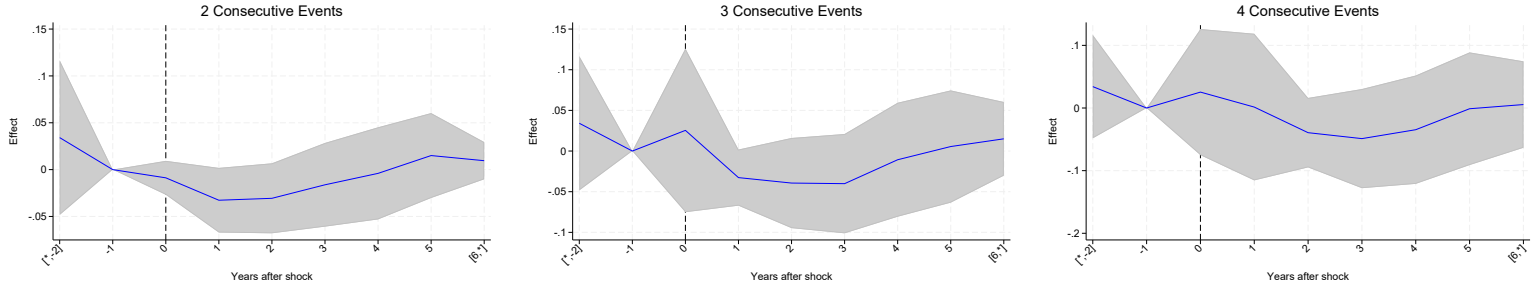

Notes: This figure reports event–study estimates of the dynamic response of Percentage Share of Build-Up to extreme–precipitation years defined using a 500mm per month threshold. All coefficients come from the event–study specification in equation (3), with district and year fixed effects and standard errors clustered at the state level. The vertical dashed line marks event time zero (the year of an extreme–precipitation year, $t = 0$); the solid blue line traces point estimates and the shaded gray band represents 95% confidence intervals. Panel (a) shows, on the left, the single–event event–study profile, and, on the right, the model–implied cumulative responses for sequences of two to four consecutive extreme–precipitation years, obtained by linearly combining the single–event coefficients under the assumption of additivity. Panel (b) disaggregates these cumulative paths by plotting separate event–study graphs for districts experiencing exactly two, three, or four consecutive shocks. See Section 2 for a full description of the data sources and Section 5 for a full discussion of the results.

Figure A5: Robustness: Event-Studies (500 mm/month) - Ln Nighlight

(a) Main plots

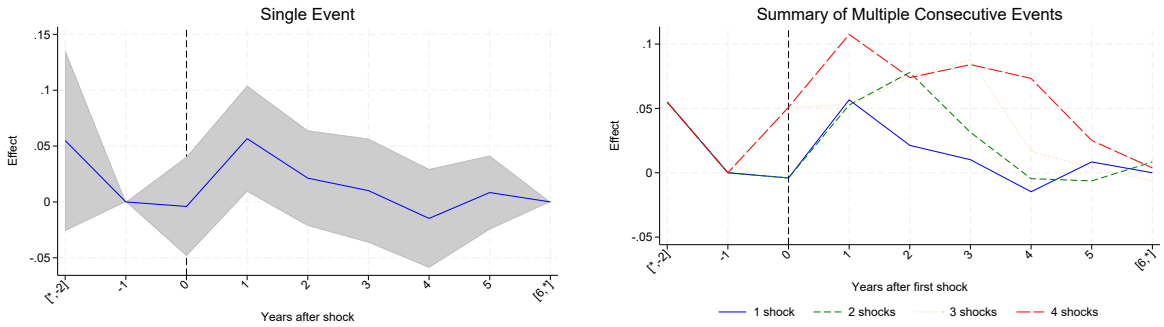

(b) Breakdown by Number of Consecutive Events

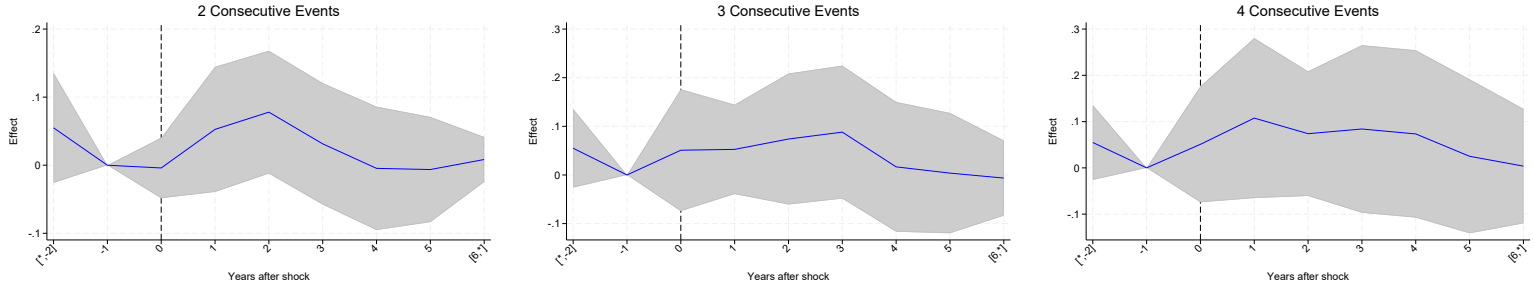

Notes: This figure reports event–study estimates of the dynamic response of Ln Nighlight to extreme–precipitation years defined using a 500mm per month threshold. All coefficients come from the event–study specification in equation (3), with district and year fixed effects and standard errors clustered at the state level. The vertical dashed line marks event time zero (the year of an extreme–precipitation year, $t = 0$); the solid blue line traces point estimates and the shaded gray band represents 95% confidence intervals. Panel (a) shows, on the left, the single–event event–study profile, and, on the right, the model–implied cumulative responses for sequences of two to four consecutive extreme–precipitation years, obtained by linearly combining the single–event coefficients under the assumption of additivity. Panel (b) disaggregates these cumulative paths by plotting separate event–study graphs for districts experiencing exactly two, three, or four consecutive shocks. See Section 2 for a full description of the data sources and Section 5 for a full discussion of the results.

School of Economics and Finance

Queen Mary
University of London

This working paper has been produced by
the School of Economics and Finance at
Queen Mary University of London

Copyright © 2025 The Author(s). All rights reserved.

School of Economics and Finance
Queen Mary University of London
Mile End Road
London E1 4NS
Tel: +44 (0)20 7882 7356
Fax: +44 (0)20 8983 3580
Web: www.econ.qmul.ac.uk/research/workingpapers/